

EE

**EUROPEAN ORGANIZATION FOR NUCLEAR RESEARCH**

**European Laboratory For Particle Physics**

CERN-SL Division

CERN LIBRARIES, GENEVA



CERN-SL-94-24

CERN SL/94-24 (AP)

SW 94 34

**DYNAMIC APERTURE**

W. Scandale

**Abstract**

Modern hadron colliders are made with high-field superconducting dipoles and quadrupoles that, in general, exhibit unintentional imperfections of the guiding field-shape due to construction tolerances, persistent currents, and saturation. Although the departure from linearity is typically small, a few units in  $10^{-4}$  at 1 cm from the axis, this phenomenon has a profound influence on the single-particle beam dynamics. The non-linear fields are at the origin of two effects: the betatron tunes change with the amplitude and the momentum of the circulating particles, and, for certain combinations of the horizontal, vertical, and synchrotron tunes, non-linear resonances are excited. As a consequence, the stability of particle motion can be considerably reduced, up to the point that the dynamic aperture can become smaller than the physical aperture of the magnets. Analytical, numerical and experimental approaches have been used to evaluate and possibly compensate mechanisms which lead to particle losses.

*Presented at the CERN Accelerator School,  
Rhodes, 20 September–1 October 1993*

Geneva, Switzerland

8 July, 1994

## C O N T E N T S

	<u>Page</u>
1. INTRODUCTION	1
2. THEORETICAL ASPECTS OF THE CONFINEMENT	1
2.1 Hamiltonian motion	1
2.1.1 Symplectic and area-preserving conditions	2
2.1.2 Eigenvalues, eigenvectors and linear stability	3
2.1.3 Liouville theorem	4
2.1.4 Canonical transformations	4
2.1.5 Poisson bracket	4
2.1.6 Poincaré mapping	5
2.2 Integrable systems	5
2.3 Non-integrable systems	8
2.3.1 The Kalmogorov–Arnold–Moser theorem	8
2.3.2 The Poincaré–Birkhoff theorem	9
2.3.3 The Chirikov criterion of overlap of the resonances	9
2.4 Definition of dynamic aperture	10
2.4.1 Phase space in an accelerator with non-linear elements	10
2.4.2 Basic procedures for confinement	12
2.4.3 Stability domain of the Hénon map	12
3. CONFINEMENT IN PARTICLE ACCELERATORS	14
3.1 Tools for dynamic aperture estimates	15
3.1.1 Transfer map for a single magnet	15
3.1.2 Tracking simulations	17
3.1.3 Maps	17
3.1.4 Early indicators of chaos	18
3.1.5 Figure of merit and data processing	19
3.2 Applications to accelerator design	21
4. REVIEW OF DEDICATED EXPERIMENTS	23
4.1 Experimental conditions	23
4.2 Results in the CERN-SPS	24
4.2.1 Short-term dynamic aperture experiment	24
4.2.2 Sextupole-induced diffusion	26
4.2.3 Effects of an external modulation of the tune	27
4.2.4 Conclusive overview of the SPS experiment	29
4.3 Results in the FNAL-Tevatron	29
4.3.1 Tune-shift, smear and short-term dynamic aperture	29
4.3.2 Particle beam trapped in resonance islands	30
4.3.3 Model for diffusion induced by sextupoles	32
4.4 Comparison of the SPS and the Tevatron experimental results	33
5. CONCLUSION	33
ACKNOWLEDGEMENTS	34
REFERENCES	35

## 1. INTRODUCTION

The original incentive to study the stability of the motion in non-linear dynamical systems is neither recent nor prompted by the necessities of accelerator design. In the second half of the last century, the development of Celestial Mechanics already provided most of the concepts that are applied nowadays to describe the orbital motion in particle accelerators. The mathematical development of this subject, which long preceded the age of computers, did in fact anticipate most of the quantitative features of non-linear dynamics, including the concept of dynamic aperture, that at present numerical simulations and experimental analysis give so much evidence for. The so-called ‘region of stochasticity’ of the phase space was in fact termed ‘region of instability’ in the late 1920s by G.D. Birkhoff [1], and the ‘homoclinic points’, around which the stochastic behaviour can be observed, were introduced in the last century by H. Poincaré [2]. The first part of my lecture will be devoted to schematically recalling the basic methods of non-linear dynamics routinely used in particle accelerators.

In the last decade, more ‘pragmatic approaches’ have been introduced by the accelerator designers to optimize the specifications and the cost of the superconducting guiding magnets for future hadron colliders [3]. Semi-analytical or purely numerical tools have been introduced to estimate the dynamic aperture as a function of various machine parameters. The effect of higher-order terms in the non-linear perturbation has been investigated with normal form techniques and related Lie algebra formalism that provide a natural generalization of the Courant–Snyder analysis for linear dynamics. On the other hand, the extraordinary progress of modern computers has made available a constantly extended numerical capacity, which allowed new simulation and analysis techniques to be explored. In the second part of this paper I shall describe how the stability of motion is investigated in modern superconducting accelerators, using as an example the case of the Large Hadron Collider (LHC) to be built in the LEP tunnel at CERN.

Despite the recent progress in understanding non-linear dynamics and in performing numerical simulations, our ability to predict the dynamic aperture in particle accelerators is quite limited. The theoretical methods available are not yet rigorously mastered, and the models for computer simulations are in general unable to include all the relevant phenomena characterizing the motion in particle accelerators. The operation of colliders may provide a wealth of information that can be exploited to reduce the gap between computer models or analytical understanding and reality. However, extracting information in full detail on non-linear dynamics from working accelerators may be extremely difficult because of the complexity inherent in their modes of operation. To overcome this difficulty, dedicated experiments have recently been performed in already well-understood hadron colliders, like the CERN–SPS or the FNAL–Tevatron, in which clear experimental conditions have been established to eliminate spurious phenomena and to bring into evidence the short-term and the long-term effect on particle motion of well-known non-linear perturbations. The third part of this paper will be devoted to a review of the main results of these experiments.

## 2. THEORETICAL ASPECTS OF THE CONFINEMENT

### 2.1 Hamiltonian motion

A  $n$ -D Hamiltonian system has  $n$  degrees of freedom and its dynamical state is represented by a point  $X$  in a  $2n$ -D phase space with generalized coordinates and momenta:

$$X = (q; p) = (q_1, p_1; q_2, p_2; \dots; q_n, p_n). \quad (1)$$

The motion is described by an Hamiltonian  $H$  and obeys Hamilton’s equations:

$$H = H(q_1, p_1; q_2, p_2; \dots; q_n, p_n; t) \quad \begin{cases} \dot{q}_i = \frac{\partial H}{\partial p_i} \\ \dot{p}_i = -\frac{\partial H}{\partial q_i} \end{cases} \quad (2)$$

The change of the Hamiltonian  $H$  with time is given by:

$$\frac{dH}{dt} = \frac{\partial H}{\partial t} + \sum_{i=1}^n \dot{q}_i \frac{\partial H}{\partial q_i} + \dot{p}_i \frac{\partial H}{\partial p_i} = \frac{\partial H}{\partial t}. \quad (3)$$

The second part of (3) comes from (2) and tells us that if the system is conservative, then  $H$  is independent of time and its value is conserved.

It has been shown by many authors [4–6] that the motion of charged particles in circular accelerators is governed by a 3-D Hamiltonian  $H(x, p_x, y, p_y, t, -E; s)$  and that the dynamical state of the particle can be represented by a point in the 6-D phase space  $(x, p_x, y, p_y, t, -E)$ , where  $(x, p_x, y, p_y)$  are the transverse coordinates and their conjugate momenta and  $(t, -E)$  is the third coordinate and its conjugate. In this representation, the independent variable of the motion is the azimuthal distance  $s$ , rather than the time  $t$ . The Hamiltonian is explicitly dependent on  $s$  and not on  $t$ , therefore the system is conservative.

It can be demonstrated in general that the motion of a system with a  $n$ -D time-dependent Hamiltonian is equivalent to that of a  $(n+1)$ -D time-independent Hamiltonian with an additional degree of freedom, expressed by the phase space variables  $(t, -E)$ .

On the other hand, a  $n$ -D time-independent Hamiltonian system can be described as a time-dependent system with  $(n-1)$ -D degrees of freedom, by choosing any generalized coordinate as the new time and the conjugate coordinate as the new time-dependent Hamiltonian.

### 2.1.1 Symplectic and area-preserving conditions

In a  $n$ -D Hamiltonian system, the Hamiltonian flow  $\mathbf{M}$  is the operator that transports points in the phase space according to Hamilton's equations. It is usual to express it in terms of a map:

$$\begin{pmatrix} Q \\ P \end{pmatrix} = \mathbf{M} \begin{pmatrix} q \\ p \end{pmatrix}. \quad (4)$$

The Jacobian  $M$  is the map linearized around one point of the phase space:

$$\text{Jacobian: } M = \begin{pmatrix} \frac{\partial(Q_1, P_1; Q_2, P_2; \dots; Q_n, P_n)}{\partial(q_1, p_1; q_2, p_2; \dots; q_n, p_n)} \end{pmatrix}. \quad (5)$$

Using Hamilton's equations it is easy to prove that the Jacobian of a Hamiltonian map obeys symplectic conditions. This has been demonstrated, in particular, for particle motion in circular accelerators [7]. The usual way to write symplectic conditions is:

$$M^T J M = J. \quad (6)$$

In the case of 2 degrees of freedom  $J$  is a  $4 \times 4$  matrix:

$$J = \begin{pmatrix} 0 & 1 & 0 & 0 \\ -1 & 0 & 0 & 0 \\ 0 & 0 & 0 & 1 \\ 0 & 0 & -1 & 0 \end{pmatrix}. \quad (7)$$

The area enclosed by a loop  $C$  of the phase space is defined as the algebraic sum of the partial areas for  $(q_i, p_i)$ . That area is also called the Poincaré integral. If the loop  $C$  moves in an Hamiltonian flow, then the Poincaré integral is an invariant of the motion and vice-versa if the area of all closed loops is conserved for all times, it is possible to find a single-valued Hamiltonian that governs the motion [8].

$$\text{Poincaré integral: } A_1 = \oint \sum_{i=1}^n p_i dq_i . \quad (8)$$

$$\text{Area-preserving } \frac{dA_1}{dt} = 0 . \quad (9)$$

### 2.1.2 Eigenvalues, eigenvectors and linear stability

The eigenvalues and the associated eigenvectors of the Jacobian  $M$  obey the equation:

$$MX = \lambda X . \quad (10)$$

The eigenvalues are the  $2n$  characteristic roots of the  $2n^{\text{th}}$  order equation for  $\lambda$ :

$$\det(M - \lambda I) = 0 \quad \text{with } I = \text{identity matrix.} \quad (11)$$

In order to have stable motion for repeated applications of  $M$ , each eigenvalue must satisfy:

$$\lim_{k \rightarrow \infty} \lambda^k = \text{bounded value} \quad \Leftrightarrow \quad |\lambda^k| \leq \rho \quad \text{with } \rho \in \mathbb{R} \text{ and } k \in \mathbb{N} . \quad (12)$$

The set of  $2n$  vectors  $X_i = (X_{ij})$  that obey Eq. (10) for the  $2n$  eigenvalues  $\lambda_i$  are the eigenvectors. They can be used to diagonalize the Jacobian  $M$ :

$$\text{Diagonalization matrix: } A = \begin{pmatrix} X_{i,j} \end{pmatrix} \quad \text{with } i, j = 1, \dots, 2n \quad (13)$$

$$\text{Diagonalized Jacobian: } \Lambda = A^{-1} M A \quad (14)$$

$$\text{Diagonalized eigenvectors: } U_i = A^{-1} X_i \quad \text{with } i = 1, \dots, 2n . \quad (15)$$

The symplectic conditions for  $M$  or  $\Lambda$  imply that eigenvalues must come in quadruples:

$$\lambda, 1/\lambda, \lambda^*, 1/\lambda^* . \quad (16)$$

Each pair  $\lambda, \lambda^*$  of eigenvalues corresponds to a normal mode of the system, i.e. a possible independent mode of behaviour.

The new Jacobian  $\Lambda$  is diagonal, and describes a linearized motion with  $n$  independent degrees of freedom.

For  $\lambda$  complex with  $|\lambda| \neq 1$  and  $\text{Im } \lambda \neq 0$ , the quadruple is symmetrical with respect to the real axis and the unit circle (case of complex instability). For  $\text{Im } \lambda = 0$ , the quadruple becomes pairs lying on the real axis (hyperbolic case). For either of these cases the linearized motion is unstable. For  $|\lambda| = 1$ , the quadruple degenerates to a pair lying on the unit circle and the linearized motion is stable (elliptic case). For  $\lambda = \pm 1$ , there is marginal stability (parabolic case).

### 2.1.3 Liouville theorem

The Liouville theorem states that the  $n$ -D Hamiltonian flow  $\mathbf{M}$  preserves the hypervolume in the  $2n$ -D phase space. This follows from the property that, in a Hamiltonian flow, the derivative of the state vector  $X$  is incompressible, i.e.:

$$\dot{X} = \left( \frac{\partial H}{\partial p_1}, -\frac{\partial H}{\partial q_1}, \dots, \frac{\partial H}{\partial p_n}, -\frac{\partial H}{\partial q_n} \right), \quad (17)$$

$$\text{div}(\dot{X}) = 0. \quad (18)$$

The Liouville theorem is important in statistical mechanics since it implies that the phase space density is invariant. It does not prevent an initially regular volume from being deformed by non-linear forces in an intricate form, imbedding a large fraction of empty space. In accelerators this phenomenon is called filamentation and for all practical purposes it implies an increase with time of the macroscopically observable region occupied by a particle beam. For instance, a kicked beam will exhibit an enlarged emittance in a profile monitor, since filled and empty parts of the phase plane are more and more intricately mixed with each other under the effect of non-linearities.

The hypervolume in the phase space can be obtained by constructing Poincaré's integral invariants of higher and higher hierarchy, the last one of which is the Liouville integral:

$$\begin{cases} A_1 = \oint \sum_{i=1}^n p_i dq_i = \iint \sum_{i=1}^n dq_i dp_i \\ A_2 = \iiint \sum_{i,k=1}^n dq_i dp_i dq_k dp_k \\ A_n = \int dq_1 dp_1 \dots dq_n dp_n \end{cases}. \quad (19)$$

The area-preserving property is equivalent to the Liouville theorem if  $n = 1$ ; it is more demanding, instead, if  $n > 1$ .

### 2.1.4 Canonical transformations

A transformation of the phase space coordinates that preserves the form of Hamilton's equations is called canonical, or symplectic, or contact transformation.

The Hamiltonian flow described by Eq. (4) is a canonical transformation.

Canonical transformations preserve area (Poincaré invariants) and hypervolume (Liouville invariant).

An important example of canonical transformation consists in changing variables into action-angle variables of the linearized motion, see for instance Ref. [5].

### 2.1.5 Poisson bracket

The Poisson bracket of two dynamical variables  $F$  and  $G$  is defined as:

$$[F, G] = \sum_{i=1}^n \frac{\partial F}{\partial q_i} \frac{\partial G}{\partial p_i} - \frac{\partial F}{\partial p_i} \frac{\partial G}{\partial q_i}. \quad (20)$$

This can be used to express in a more compact form the Hamilton's equations and the evolution of a dynamical variable with time:

$$\begin{cases} \dot{q}_i = [q_i, H] \\ \dot{p}_i = [p_i, H] \end{cases} \quad (21)$$

$$\dot{F} = [F, H] + \frac{\partial F}{\partial t} . \quad (22)$$

The Poisson brackets obey the following fundamental relations:

$$[q_i, q_j] = 0 \quad [p_i, p_j] = 0 \quad [q_i, p_j] = \delta_{ij} \quad (23)$$

$$\text{Jacoby identity: } [A, [B, C]] + [B, [C, A]] + [C, [A, B]] = 0 . \quad (24)$$

Using Eqs. (23) and (24) it is possible to define a Lie algebra structure on the space of Hamiltonian vector fields [8] and to represent a Hamiltonian flow as a Lie series:

$$\mathcal{M} X = e^{:H:X} = \sum_{i=1}^{\infty} (:H:)^i \frac{X}{i!}, \quad (25)$$

where the operator  $:H:$  is defined in terms of Poisson brackets of the Hamiltonian:

$$\left\{ \begin{array}{l} :H:X = [H, X] \\ (:H:)^2 X = [H, [H, X]] \\ \dots \\ (:H:)^i X = \underbrace{[H, [H, \dots, [H, X]]]}_{i \text{ times}} \end{array} \right. \quad (26)$$

### 2.1.6 Poincaré mapping

A natural way to correlate Hamiltonian flows and discrete maps is based on the concept of surface of section introduced by Poincaré [2].

In a  $n$ -D time-independent Hamiltonian system, the total energy  $H$  is conserved and this confines the motion in a so-called energy shell of the phase space, that is a  $(2n-1)$ -D set of the phase space. On the energy shell one of the phase space coordinates, say the momentum  $p_n$ , can be expressed as a function of the other coordinates, since:

$$H(q, p) = E_0 . \quad (27)$$

The condition  $q_n = \text{constant}$  identify a  $(2n-2)$ -D surface in the energy shell, that represents a surface of section for the trajectory. The successive intersections of the trajectory with the surface of section define the Poincaré map that iteratively correlates points in the reduced phase space  $(q_1, p_1; \dots; q_{n-1}, p_{n-1})$ . The Liouville theorem implies that hypervolume in the reduced phase space is conserved. If additional independent invariants of motion exist, the Poincaré section will lie on a surface of dimensionality less than  $(2n-2)$ -D, otherwise it will fill densely a bounded region of the  $(2n-2)$ -D phase space. Projections of the surface of section into the  $n-1$  phase planes  $(q_i, p_i)$ , with  $i = 1, \dots, n-1$ , are a useful way to visualize the motion. Separable Hamiltonians for the phase coordinates  $q_i, p_i$  imply area-preserving motion in the  $(q_i, p_i)$  phase plane and trajectory intersections lying on a smooth curve. Non-separable Hamiltonians, instead, generally produce annular shapes of finite area in any  $(q_i, p_i)$  phase plane projection.

In particle accelerators, intersections of 6-D trajectories with  $H = E_0$  and  $t = k \cdot T$ , where  $T$  is the revolution period, provide the Poincaré map of the transverse motion at a given azimuthal position. The condition  $t - t_0 = \text{constant}$ , where  $t_0$  is the time of arrival of the synchronous particle, say at the location of the RF cavity, provides a stroboscopic view of the transverse motion with the synchrotron frequency.

## 2.2 Integrable systems

A  $n$ -D dynamical system is integrable if it has  $n$  independent integrals of motion, i.e., in  $2n$ -D action-angle phase space, the Hamiltonian has the general form:

$$H(J, \theta) = H_0(J) \quad \text{with } J = (J_1, \dots, J_n) \quad \text{and } \theta = (\theta_1, \dots, \theta_n) . \quad (28)$$

The  $n$  actions  $J_i$ , with  $i = 1, \dots, n$ , are the  $n$  invariants from which the energy conservation can be deduced. Each action invariant reduces by one the dimensionality of the phase space set that contains the trajectory. The overall motion is thereby confined to a  $n$ -D invariant torus parametrized by the  $n$  action variables, on which the  $n$  angle variables run.

Rigorously speaking, invariant tori exist under the condition that the  $n$  integrals of motion be independent and in involution [8], that is, the following relations hold for all  $i$  and  $j$ :

$$\left\{ \begin{array}{ll} [H, J_i] = 0 & \text{invariance of } J_i \\ [J_i, J_j] = 0 & J_i, J_j \text{ in involution} \\ \sum_{i=1}^n a_i dJ_i = 0 \Rightarrow (a_1, \dots, a_n) = 0 & J_1, \dots, J_n \text{ independent} \end{array} \right. \quad (29)$$

For each pair of conjugate coordinates  $(\theta_i, J_i)$  the motion is  $2\pi$ -periodic for  $\theta_i$  and follows closed curves, topologically equivalent to circles. The frequency of each mode is:

$$\omega_i(J_1, \dots, J_n) = \frac{\partial H}{\partial J_i}(J_1, \dots, J_n) . \quad (30)$$

A resonance occurs when the frequencies  $\omega_i$  are rationally related by a set of  $n$  integers  $s_i$  not all equal to zero:

$$\sum_{i=1}^n s_i \omega_i = 0 . \quad (31)$$

In the generic non-resonant case, the trajectory is dense on the torus, i.e. it passes arbitrarily close to every point of the torus.

In the resonant case the trajectory closes onto itself after  $s_i$  revolutions of the phase  $\theta_i$ , i.e. it is a periodic orbit, and the invariant torus degenerates into invariant tori of lower dimension. Since the integers  $s_i$  can be arbitrarily large, there are periodic orbits arbitrarily close to one another in action space.

In each  $(\theta_i, J_i)$  phase plane, the Poincaré section of a resonant trajectory is a set of  $s_i$  parabolic fixed-points that depends on the initial condition of the angle. All of them lie on a circle parametrized by the resonant action invariant.

For non-linear systems there are trajectories with resonant frequency arbitrarily close to any trajectory with non-resonant frequency. This means that for an arbitrarily small change of the initial conditions, an orbit can move from a non-degenerate to a degenerate torus. This ‘structural instability’ plays the role of the devil in non-linear dynamics.

A simple example of a 2-D integrable system that performs linear motion is the time-independent oscillator with uncoupled degrees of freedom described by the Hamiltonian

$$H_0(J) = \omega_1 J_1 + \omega_2 J_2 . \quad (32)$$

An example of a non-linear system is the oscillator with amplitude-dependent frequencies described by the Hamiltonian:

$$H_0(J) = H_1(J_1) + H_2(J_2) . \quad (33)$$

The solution of the Hamilton equations is:

$$\begin{cases} \theta_1(t) = \theta_1(0) + \frac{\partial H_1(J_1)}{\partial J_1} t = \theta_1(0) + \omega_1(J_1)t \\ \theta_2(t) = \theta_2(0) + \frac{\partial H_2(J_2)}{\partial J_2} t = \theta_2(0) + \omega_2(J_2)t \end{cases} \quad (34)$$

The projection for  $t$  integer provides the so-called twist map:

$$\begin{cases} J_{1,k+1} = J_{1,k} \\ \theta_{1,k+1} = \theta_{1,k} + 2\pi\alpha(J_{1,k+1}) \\ J_{2,k+1} = J_{2,k} \\ \theta_{2,k+1} = \theta_{2,k} + 2\pi\alpha(J_{2,k+1}) \end{cases} \quad (35)$$

Invariant tori and their Poincaré projections in the phase plane  $(\theta_1, J_1)$  for case (35) are illustrated in Fig. 1. Assuming given values of  $J_1$  and  $J_2$ , the rotational frequencies and their ratio  $r$  are also fixed:

$$\begin{cases} \omega_1 = \omega_1(J_1) = 2\pi\alpha(J_1) \\ \omega_2 = \omega_2(J_2) = 2\pi\alpha(J_2) \\ r = \frac{\omega_1}{\omega_2} \end{cases} \quad (36)$$

For  $r$  irrational, the trajectory maps onto the entire torus surface and its projection maps onto the circle of radius  $J_1$ . For  $r$  rational, the torus degenerates into a closed curve and its section is a finite set of fixed points.

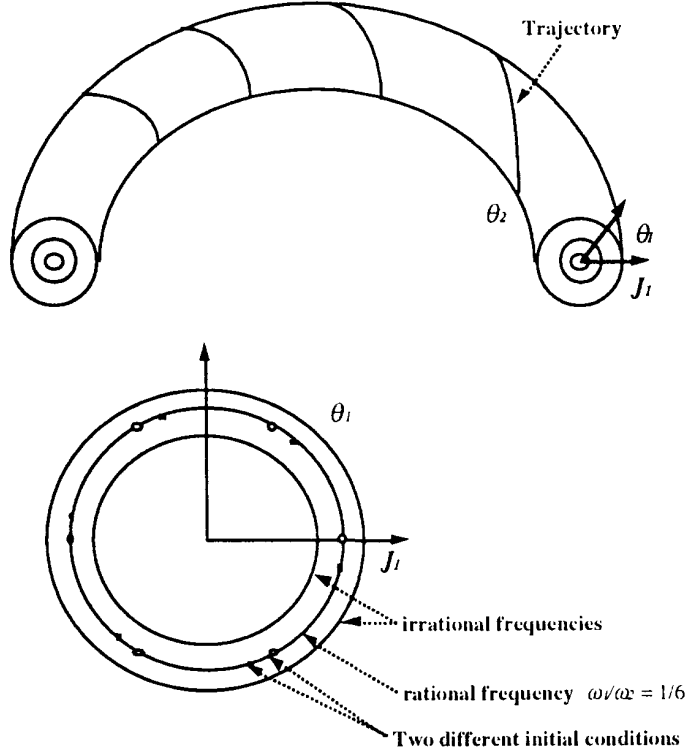


Fig. 1: Motion of an integrable system with two degrees of freedom.

Upper part: the motion lies on a torus  $J_1 = \text{const. } J_2 = \text{const.}$

Lower part: Poincaré surface of section after a large number of trajectory intersections.

## 2.3 Non-integrable systems

A  $n$ -D integrable system slightly perturbed in such a way that the Hamiltonian is also a function of the angles is, in general, non-integrable. Its Hamiltonian has the general form:

$$H(J, \theta) = H_0(J) + \epsilon H_1(J, \theta). \quad (37)$$

The perturbation term  $\epsilon H_1(J, \theta)$  produces non-linear coupling and resonances among degrees of freedom, so that, near resonances, the regular solutions are strongly perturbed while the trajectories in the phase space undergo a change in topology. The singularity can be removed at an isolated resonance by an appropriate canonical transformation, as described for instance in Ref. [9] for particle dynamics.

However, in a non-integrable system, the general problem of the confinement requires deep investigations on the interaction between resonances and on the existence and accessibility of invariant sets in the phase space.

### 2.3.1 The Kalmogorov–Arnold–Moser theorem

The Kalmogorov–Arnold–Moser (KAM) theorem states that in a  $n$ -D system with the Hamiltonian (37) some of the invariant tori of the unperturbed motion are preserved under sufficiently small and smooth perturbations, provided there is a sufficiently large non-linearity. Those invariant tori are preserved that are sufficiently far from all resonances in units of resonance width.

The perturbed torus is parametrized by  $n$  phase variables  $\phi = (\phi_1, \dots, \phi_n)$  and by  $\epsilon$ :

$$\begin{cases} J = I + V(\phi, \epsilon) \\ \theta = \phi + U(\phi, \epsilon) \end{cases} \quad (38)$$

$U$  and  $V$  are periodic functions in  $\phi$  that vanish for  $\epsilon = 0$ , in which case,  $\phi$  coincides with  $\theta$ , the unperturbed phase of the motion.

The requirement of a sufficient non-linearity implies that, in the vicinity of non-resonant points of the phase space, there be some domain of  $J$  where the eigenfrequencies are linearly independent, or non-resonant:

$$\sum_{i=1}^n s_i \omega_i \neq 0 \quad \text{with} \quad \omega_i = \frac{\partial H_0}{\partial J_i}. \quad (39)$$

In the neighbourhood of resonances the perturbation induces a distortion of the orbit, and a variation of the action, which in turns modifies the frequency and brings the system out of resonance. This mechanism limits the overall change of the perturbed action and eventually allows perturbed KAM tori to stay in the vicinity of the unperturbed invariants. Since there are an infinite number of resonances, which approach sufficiently close to any point in the phase space, invariant tori are preserved far from low-order resonances provided the width of the neighbouring higher-order resonances converges sufficiently rapidly with the order  $s$  of the resonance. This requires the perturbing part of the Hamiltonian to be sufficiently smooth and differentiable for higher-order terms of the Fourier expansion to be small.

KAM invariants have diophantine frequencies:

$$|\vec{s} \cdot \vec{\omega}| \geq \gamma |\vec{s}|^{-\eta} \quad \text{with} \quad \vec{s} = (s_1, \dots, s_n), \quad \vec{\omega} = (\omega_1, \dots, \omega_n), \quad (40)$$

with  $\gamma$  and  $\eta$  positive constants, the first depending on  $\epsilon$ , the second on  $n$ .

Therefore, for increasing values of the perturbation, KAM invariants persist for those irrational frequencies that are hardest to be approximated by rational ones. The Chirikov criterion discussed below will clarify this point in terms of resonances and resonance width.

The KAM theorem, called in this form in recognition of the work of Kolmogorov, Arnold and Moser in the 1950s and 1960s, has an exceedingly small range of validity, which prevents any quantitative application to physical systems and in particular to beam dynamics in particle accelerators. However, its proof brings to our attention the crucial assessment that regular motion can be observed with certain restrictions also in non-integrable systems.

### 2.3.2 The Poincaré–Birkhoff theorem

The Poincaré–Birkhoff theorem applies to 2-D non-integrable systems and gives a deep insight on the breaking mechanism of invariant curves.

Let us consider as an example the 2-D oscillator with amplitude-dependent frequencies described by the Hamiltonian (33), to which a small non-integrable perturbation is added. The surface of section with  $H = E_0$  and  $\theta_2 = \text{constant}$ , identify a Poincaré map. The unperturbed motion is characterized by the ratio  $r$  of the two linearized frequencies, in particular, rational values of  $r$  characterize fixed points of the map:

$$r(J_1, J_2) = \frac{\omega_1}{\omega_2} = \frac{q}{s}. \quad (41)$$

Equations (41) identify a circle of fixed points of order  $s$ , in the phase plane  $(\theta_1, J_1)$ .

The Poincaré–Birkhoff theorem states that generically  $2s$  of them survive the perturbation and appear in chains of alternating elliptic and hyperbolic fixed points. Regular phase space trajectories encircle the elliptic points and a separatrix trajectory connects the hyperbolic points. The typical pattern is that of a chain of islands. Orbits in the neighbourhood of elliptic fixed points in general reveal higher-order resonances and fixed points which have similar characteristics to those just analysed above, but on a finer scale. The driving term is proportional to  $1/s!$ , the order of the considered resonance. Orbits in the vicinity of hyperbolic fixed points are the connection of four curves, two of them are incoming separatrices, the two others are outgoing separatrices. Incoming and outgoing separatrices interconnect the set of hyperbolic fixed points of a resonance. The movement along the separatrices becomes increasingly slow as an hyperbolic fixed point is approached. Incoming and outgoing separatrices intersect each other in an intricate way, and in the vicinity of hyperbolic fixed points the number of the intersections, also called homoclinic points, diverges to infinity. In addition, along the separatrix there is an infinity of secondary resonances corresponding to multiples of  $s$ . Each secondary resonance has its own set of alternating elliptic and hyperbolic points, and its own separatrices. Separatrices of primary and secondary resonances in general follow wild trajectories that intersect each other in heteroclinic points. Homoclinic and heteroclinic points fill densely the space surrounding the circle of fixed points of the unperturbed system, characterized by Eq. (41). In that region KAM tori cannot exist: the phase-space trajectory is generically stochastic, since it changes topology at each singularity crossing. The size of the stochastic region around the separatrix grows as the perturbation amplitude increases, however, there is not an abrupt transition to stochasticity for some critical value of the perturbation.

### 2.3.3 The Chirikov criterion of overlap of the resonances

Chains of resonant islands have a characteristic width that increases with the perturbation strength and that can be approximately estimated by an appropriate expansion technique [9]. For small perturbations, neighbouring chains of different order resonances are eventually well separated and can be described as isolated resonances. Chirikov suggested [10] that the largest perturbation parameter for which adjacent primary chains of islands overlap is a good estimate for the value of the perturbation required to destroy the last KAM invariant between these islands. This criterion has an intuitive appeal, since we already know that regions around separatrices are in fact stochastic, therefore we cannot expect regular motion in between two chains of resonances whose separatrices intersect each other.

However, the above criterion is too severe a condition for stochasticity. In fact, the last KAM torus is destroyed well before resonance overlapping occurs, because of the interaction between the two primary resonances that modify the topology of the phase space, and because of the existence of secondary resonances lying between the primary ones.

The criterion has to be used with care since higher-order perturbations may have to be estimated to find the appropriate resonance width. Whenever it holds, there is a transition from local to global stochasticity. In other terms, stochastic areas surrounding isolated islands become interconnected over a large fraction of the phase space, where the motion is no longer regular.

## 2.4 Definition of dynamic aperture

Rigorously speaking, the dynamic aperture is the innermost radius of the region in the phase space, where the motion is stable. Trajectories with initial conditions in this domain remain confined for ever. Posed in this form, the question of the stability of the motion can only be tackled by a purely mathematical approach that apparently has little if any practical significance. The kind of stability we are talking about can be defined as follows:

$X(t)$  is stable if for all  $t$  and for any  $\varepsilon > 0$  there is a  $\delta > 0$  such that:

$$|X(0)| < \delta \quad \Rightarrow \quad |X(t)| < \varepsilon . \quad (42)$$

For practical applications the concept of confinement has to be defined within an appropriate time scale. In particle accelerators, two regimes of interest can be identified in terms of the number of stable revolutions along the ring.

The short-term dynamic aperture requires confinement for  $10^3$  to  $10^4$  revolutions. This is relevant for transient phenomena such as the injection process or beam observations. At injection, the initially large amplitude of oscillation due to steering errors is in general reduced with feed-back devices: confinement at large amplitude for about a damping time is thus sufficient to avoid particle losses. On the other hand, dedicated experiments are generally planned to explore the phase-space parameters as a function of the amplitude. Measurements, which in general require up to a few thousand turns, can be performed up to the short-term dynamic aperture.

The long-term dynamic aperture instead concerns steady-state regimes lasting  $10^7$  to  $10^9$  revolutions, like injection or collision plateaux.

Phenomena that cannot be treated by Hamiltonian mechanics, like external noise, dissipation, quantum effect, and gas scattering in general play an essential role in the investigation of short-term and long-term dynamic aperture. Nevertheless, the abstract problem of the Hamiltonian confinement has a strong significance for the practical confinement.

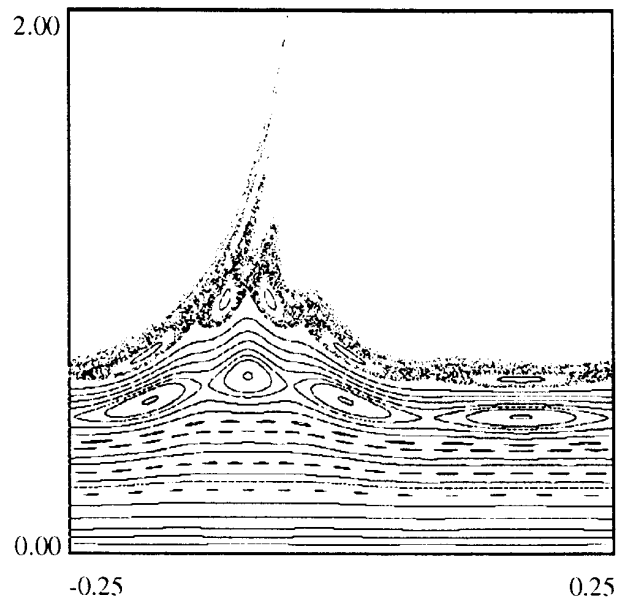
### 2.4.1 Phase space in an accelerator with non-linear elements

In a linear machine with irrational tunes the motion is stable and regular all around the closed reference orbit near the magnetic axis.

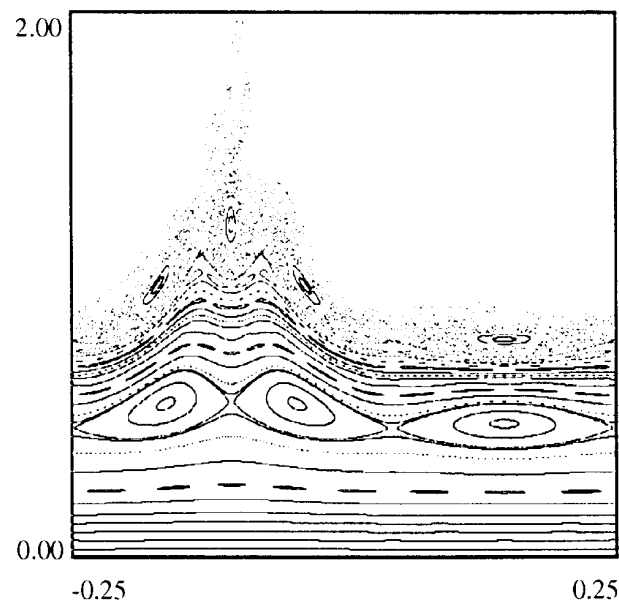
The non-linear fields add a tune dependence with the amplitude, which shifts tunes to rational values, provoking resonant phenomena accompanied in the phase space by islands of finite area surrounded by thin chaotic layers. The islands and the chaotic layers exist throughout the entire phase space. However, at small amplitude, trajectories follow invariant surfaces, the KAM tori, and remain stable for indefinite time. As the amplitude increases, the islands become larger until they overlap. Analytically the chaotic limit is well defined for phenomena with 2-D Hamiltonian only since, in these cases, the domain with regular motion is foliated in 2-D tori that encircle the origin and any existing layer of isolated higher-order resonances. When the resonances overlap, the chaotic layers become interconnected and the particle motion is no longer bounded. With more degrees of freedom, the tori have higher dimensions and therefore no longer form an impassable barrier. Particles in stochastic layers, even close to the origin, may escape through the entire phase space, owing to the so called Arnold diffusion. However, for all practical purposes, the border between mostly regular and mostly chaotic trajectories still exists and defines the long-term dynamic aperture. The confinement inside this border requires weak perturbations and is limited by local-scale stochasticity. Outside the long-term dynamic aperture, the motion is globally stochastic until, for some value of the amplitude, a separatrix going to infinity is encountered that makes the motion totally unstable. Particles with initial conditions in the large-scale stochastic area have

totally erratic trajectories; however, they generally survive for a decreasing number of turns as the initial amplitude increases. The short-term dynamic aperture is the border of the region where the survival time is still comparable to the duration of transient phenomena in particle accelerators.

The topological properties of the phase space described here are pictorially illustrated in Fig. 2.



a) Betatron frequency near the 1/6 resonance



b) Betatron frequency near the 1/5 resonance

Abscissa: angular coordinate in units of  $2\pi$   
Ordinate: action coordinate in arbitrary units

Fig. 2: Phase space topology of a non-linear system.

### 2.4.2 Basic procedures for confinement

The resonances play a crucial role for both theoretical and practical confinement problems. Therefore the basic step to finding dynamic apertures requires the careful identification of all the resonances near the working region of interest in the phase space.

The basic way to enlarge the dynamic aperture is to reduce as much as possible the resonance strength, i.e. to make as small and as smooth as possible the perturbing non-linear terms.

In particular, reducing the strength of low-order resonances and choosing the working eigenfrequencies far from them increases the short-term dynamic aperture. Smearing out the perturbation reduces the width of higher-order resonances, and increases the stability domain.

Residual external noise produces unwanted modulations of the eigenfrequencies and satellite resonances which in turn enlarge the stochastic area close to separatrices and reduce the threshold for overlapping criterion. Powerful noise reduction methods are needed to improve confinement.

### 2.4.3 Stability domain of the Hénon map

The Hénon map [11] is a simple 1-D non-linear system that can be used to illustrate some of the concepts relative to confinement. In terms of accelerator physics, the Hénon map corresponds to the horizontal motion in a FODO cell with one sextupole, in thin-lens approximation.

The Hamiltonian is:

$$H(x, p, s) = \omega^2 \frac{x^2}{2} + \frac{p^2}{2} - \omega \frac{x^3}{3} \sum_{k=-\infty}^{\infty} \delta(s - k\ell) \quad \text{with} \quad \frac{\omega}{2\pi} \in \left[0, \frac{1}{2}\right], \quad (43)$$

where  $\omega$  is the frequency of the linearized motion and  $\ell$  is the length of the cell.

The equations of motion are:

$$\begin{cases} \dot{x} = p \\ \dot{p} = -\omega^2 x + \omega x^2 \sum_{n=-\infty}^{\infty} \delta(s - n\ell). \end{cases} \quad (44)$$

The Hénon map solves them iteratively turn after turn:

$$\begin{pmatrix} x_{k+1} \\ p_{k+1} \end{pmatrix} = R(\omega T) \begin{pmatrix} x_k \\ p_k \end{pmatrix} + \begin{pmatrix} 0 \\ x_k^2 \end{pmatrix} \quad \text{with} \quad R(\omega t) = \begin{pmatrix} \cos \omega t & \sin \omega t \\ -\sin \omega t & \cos \omega t \end{pmatrix}; \quad (45)$$

where  $x_k, p_k$  are the position and the conjugate momentum, respectively, at the location  $\ell$  and at the times  $k \cdot T$ , where  $T$  is the transit time through the cell.

Introducing normalized coordinates  $\bar{x}_k = x_k, \bar{p}_k = p_k/\omega$ , and assuming  $T$  as the unit time, the linearized part of the Hénon map can be expressed as:

$$L_k \begin{pmatrix} \bar{x}_k \\ \bar{p}_k \end{pmatrix} = R(\omega) \begin{pmatrix} 1 & 0 \\ 2\bar{x}_k & 1 \end{pmatrix} \circ \begin{pmatrix} \bar{x}_k \\ \bar{p}_k \end{pmatrix}. \quad (46)$$

The Hénon map (45) has two fixed points, one of which is the origin:

$$\begin{pmatrix} \bar{x}_S \\ \bar{p}_S \end{pmatrix} = \begin{pmatrix} 0 \\ 0 \end{pmatrix}, \quad \begin{pmatrix} \bar{x}_U \\ \bar{p}_U \end{pmatrix} = \begin{pmatrix} 2 \tan \frac{\omega}{2} \\ -2 \tan^2 \frac{\omega}{2} \end{pmatrix}. \quad (47)$$

From the inspection of the trace of  $L$ , the origin is found to be stable and the second fixed point unstable, for any value of the frequency.

$$\text{Tr}(L_k) = 2\cos\omega + 2\bar{x}_k \sin\omega \Rightarrow \begin{cases} \text{Tr}(L_{\bar{x}_k=\bar{x}_S}) = 2\cos\omega \in [-2, +2] \Rightarrow \text{stable} \\ \text{Tr}(L_{\bar{x}_k=\bar{x}_U}) = 2 + 4\sin^2\left(\frac{\omega}{2}\right) \in [2, 6] \Rightarrow \text{unstable} \end{cases} \quad (48)$$

The phase space portrait resulting from the iteration of the Hénon map exhibits complicated structures, as in Fig. 3, where the eigenfrequency is chosen in the vicinity of the fourth-order resonance. The dashed area around the origin and inside the four resonant islands is stable. The winding curve that encircles the stable area is the separatrix, obtained by iterating repeatedly a point initially close to the unstable fixed point. A large multitude of homoclinic points appears, that announces chaotic motion. Above the separatrix the motion is unstable. Chains of higher-order islands are visible as the phase space is explored at a finer scale, as in Fig. 4, where the eigenfrequency is chosen in the vicinity of the fifth-order resonance.

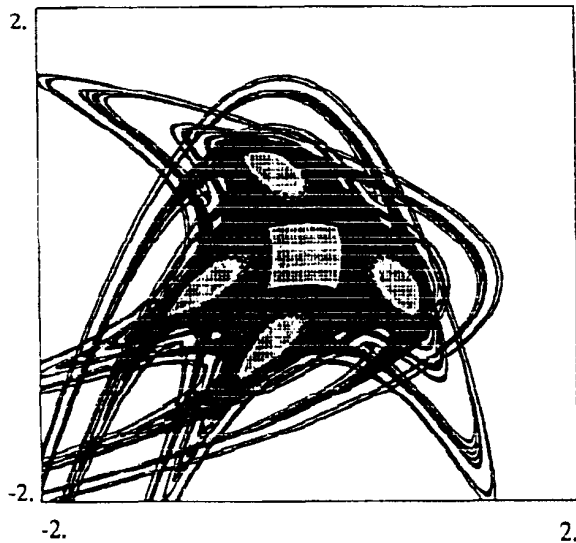


Fig. 3: Phase space portrait of the Hénon map near the 1/4 resonance.

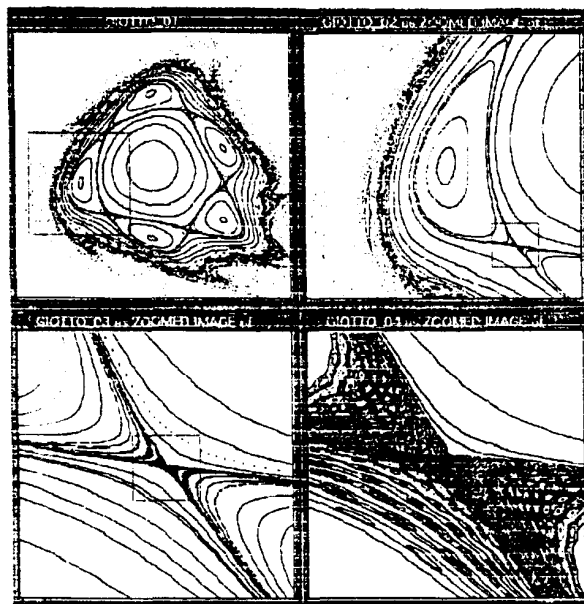


Fig. 4: Phase space portrait of the Hénon map near 1/5 resonance.

The standard way to find the dynamic aperture requires iteration of an appropriate number of the Hénon map for increasing values of the initial amplitude [12]. The domain of stability generally shrinks as the eigenfrequency approaches rational values, as in Fig. 5.

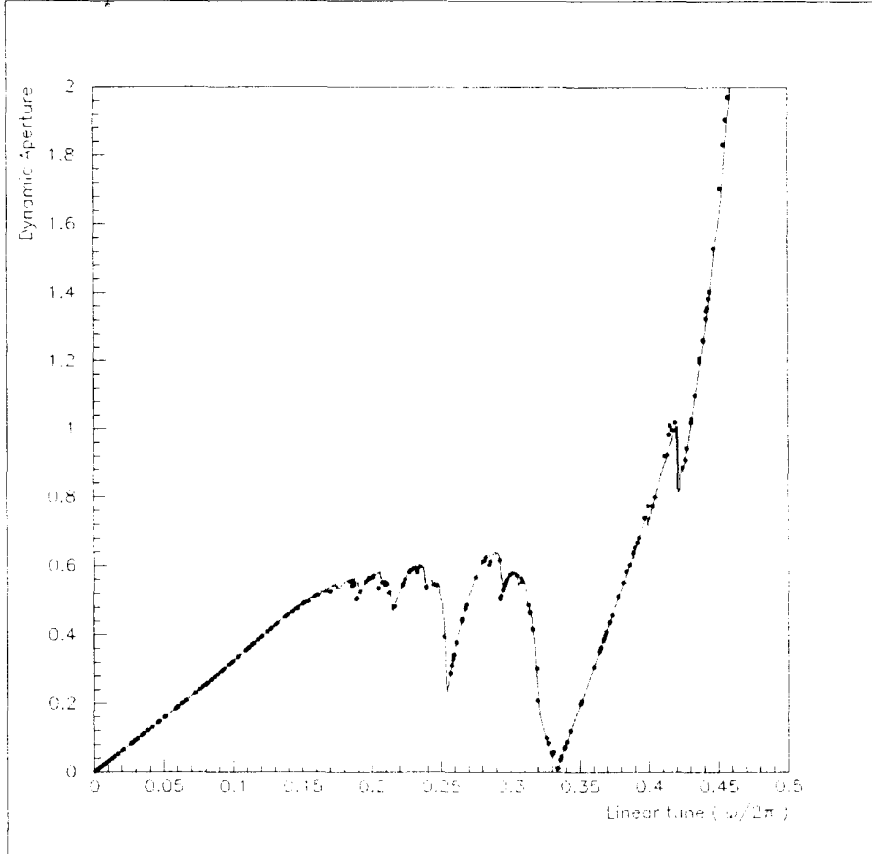


Fig. 5: Dynamic aperture of the Hénon map

### 3. CONFINEMENT IN PARTICLE ACCELERATORS

The motion of charged particles in circular accelerators is basically governed by the magnetic field of the guiding dipoles and the focusing quadrupoles. Intentional and non-intentional non-linear fields are in general also present, the side-effect of which is to induce losses at large amplitude. Sextupoles are used to reduce the chromaticity, and octupoles make the tune dependent on the amplitude, which is sometime exploited to improve the current-dependent behaviour. In hadron accelerators, the destabilizing action of chromaticity sextupoles is self-compensated to a large extent due to the regularity of the lattice. However, a strongly focused lattice is usually necessary to reduce the sensitivity to field errors, and this in turn increases the strength of chromaticity sextupoles. Unintentional multipoles due to unavoidable imperfections of the guiding and focusing fields introduce additional non-linearities, which represent the greatest hazard. Longitudinal fringeing fields, instead, play a non-negligible role in small machines only, therefore, hard-edge representation of the magnetic fields along the azimuth is considered a valid approximation for large accelerators. The situation can be very different for different machine types. For instance, in modern electron accelerators, the chromatic aberration is even larger, due to the stronger focusing required to reduce the transverse beam size. Consequently, sophisticated sextupole corrector schemes are used, that include elements in zero-dispersion regions to partly compensate resonances, whilst strongly non-linear insertion devices, like wigglers and undulators, are often present.

Practical methods to study the confinement have to be adapted to the specific case under investigation. It is outside of the scope of this lecture to give an exhaustive overview of the

known problems and of the proposed solutions. Instead, we will limit ourselves from now on to discussing the confinement in large hadron accelerators with superconducting magnets, even if some of the concepts illustrated in this section are of a more general and wider applicability.

In hadron colliders of the new generation, compromises must be found between making magnetic fields as uniform as possible and keeping magnet costs low. This is a difficult challenge for superconducting magnets, whose quality depends on the mechanical tolerances of the coil geometry, rather than on the shape of the poles. Both in the Tevatron and in the Hera magnets, typical deviations from uniformity have been limited to about one part in ten thousand at 2.5 centimetres from the magnet axis. Similar values, properly extrapolated with the inner coil diameter and the superconducting filament size, are expected to be reached in the magnets of the SSC, the LHC, and RHIC. Much smaller imperfections are in general present in warm magnets.

The single-particle approach provides a sufficiently simple, reliable, and coherent model of the real accelerator to investigate performances related to non-linear dynamics. The key issue is to estimate the stability of the motion over the operational cycle of the accelerator. Both analytical and numerical tools are used to estimate the dynamic aperture as a function of various machine parameters. Improvements of the linear lattice and correction schemes are studied to reduce the influence of the non-linear forces, and to specify upper limits for the magnet imperfections. The final validation is, in general, performed with numerical simulations in which the particle position is tracked element by element around the machine for large numbers of turns. In this section two subjects are reviewed: the tools by which predictions on beam stability are formulated, and the applications on accelerator design.

### 3.1 Tools for dynamic aperture estimates

In hadron accelerators non-linear problems are usually addressed for 2-D transverse degrees of freedom, neglecting the coupling with longitudinal motion. For numerical studies and computer tracking simulations, more realistic 3-D models are preferred.

#### 3.1.1 Transfer map for a single magnet

Charged particles travelling through linear magnets obey the 2-D equations of motion:

$$\frac{d\vec{z}}{ds} + K(s)\vec{z} = 0, \quad (49)$$

with:

$$\vec{z}(s) = \begin{pmatrix} z_1(s) \\ z_2(s) \\ z_3(s) \\ z_4(s) \end{pmatrix} = \begin{pmatrix} x(s) \\ p_x(s) \\ y(s) \\ p_y(s) \end{pmatrix}, \quad K(s) = \begin{pmatrix} 0 & 1 & 0 & 0 \\ k_1(s) + \rho^{-2}(s) & 0 & 0 & 0 \\ 0 & 0 & 0 & 1 \\ 0 & 0 & -k_1(s) & 0 \end{pmatrix}. \quad (50)$$

In single dipoles or quadrupoles,  $K$  is constant with respect to  $s$ , therefore Eq. (41) can be analytically solved piece-wise, see for instance Ref. [13]. The solution is in general expressed as a linear transport matrix  $L$ , that obeys the usual composition rules:

$$\vec{z}(s) = L(s, s_0) \vec{z}(s_0), \quad (51)$$

$$L(s_0, s_0) = I, \text{ the identity map}, \quad (52)$$

$$L(s_1, s_0) = L(s_1, s) \circ L(s, s_0). \quad (53)$$

The matrix  $L$  also satisfies the linear equation:

$$\frac{dL(s, s_0)}{ds} = K(s) \circ L(s, s_0) , \quad (54)$$

the general solution of which can be written as:

$$L(s_0 + \ell, s_0) = e^{\ell K} = \sum_{i=0}^{\infty} \ell^i \frac{K^i}{i!} . \quad (55)$$

In an extended multipolar magnet with non-linear field-shape components a forcing term is present in the equation of motion.

$$\frac{d\vec{z}}{ds} + K(s)\vec{z} = \vec{f}(x, y; s) \quad \text{with} \quad \vec{f}(x, y; s) = \begin{pmatrix} 0 \\ f_x(x, y; s) \\ 0 \\ f_y(x, y; s) \end{pmatrix} . \quad (56)$$

The perturbation  $\vec{f}(x, y; s)$  is expressed in terms of normal and skew multipolar strengths up to order  $m$ , called  $k_l$  and  $j_l$  respectively, that correspond to the relative field-shape deviations  $b_l$  and  $a_l$ , respectively, measured at a distance  $R$  from the magnetic axis.

$$\begin{cases} f_x(x, y; s) = \operatorname{Re} \left[ \sum_{l=2}^m \frac{1}{l!} (k_l + i j_l) (x + iy)^l \right] = \operatorname{Re} \left[ B_0 \sum_{l=2}^m (b_{l+1} + ia_{l+1}) \left( \frac{x+iy}{R} \right)^l \right] \\ f_y(x, y; s) = -\operatorname{Im} \left[ \sum_{l=2}^m \frac{1}{l!} (k_l + i j_l) (x + iy)^l \right] = -\operatorname{Im} \left[ B_0 \sum_{l=2}^m (b_{l+1} + ia_{l+1}) \left( \frac{x+iy}{R} \right)^l \right] \end{cases} \quad (57)$$

In general, Eq. (56) cannot be analytically solved. Approximate solutions can be found, instead, either by neglecting higher-order contributions to the particle trajectory, or by localizing the entire non-linear content of the multipolar components in a few points along the azimuth.

In the first approach, called thick-lens approximation, approximate trajectories are found across extended magnets by a recursive method, which initially starts from the linear approximation:

$$\begin{cases} \vec{z}_1 = L(s, s_0) \vec{z}(s_0) = L(s, s_0) \vec{z}_0 \\ \vec{z}_k(s) = L(s, s_0) \vec{z}_{k-1}(s_0) + \int_{s_0}^s L(s', s_0) \vec{f}[x_{k-1}, y_{k-1}; s'] ds' . \end{cases} \quad (58)$$

At each step  $k$ , the final coordinates are expressed as a polynomial expansion of order  $k$  in the initial conditions. The resulting map is called the Taylor map of order  $k$ :

$$z_{j,k}(s_0 + \ell) = \sum_{i=1}^k \sum_{(i_1+i_2+i_3+i_4)=i} c_{j;i_1,i_2,i_3,i_4} z_1^{i_1}(s_0) z_2^{i_2}(s_0) z_3^{i_3}(s_0) z_4^{i_4}(s_0) \quad \text{for } j = 1, \dots, 4. \quad (59)$$

At the order  $k$ , the symplectic conditions (6) are violated by terms of order  $|\vec{z}(s_0)|^{k+1}$ .

The second approximation method for solving Eq. (56) is based on the assumption that the non-linear perturbation is concentrated in one or more locations inside the magnet. Usually, the non-linearity is localized in the middle of the magnetic length:

$$\vec{f}(x, y; s) = \vec{f}(x, y; s) \ell \delta(s - s^*) \quad \text{with} \quad s^* = s_0 + \frac{\ell}{2} . \quad (60)$$

The transfer map, also called the thin-lens approximation, becomes:

$$\vec{z}(s_0 + \ell) = \mathbf{K}(s^*)\vec{z}(s_0) \Leftrightarrow \begin{cases} \vec{z}(s^*) = \mathbf{L}(s^*, s_0)\vec{z}(s_0) \\ \vec{z}(s_0 + \ell) = \mathbf{L}(s_0 + \ell, s^*)[\ell \vec{f}(x^*, y^*; s^*) + \vec{z}(s^*)] \end{cases}. \quad (61)$$

Terms of the order of  $\ell^2/\rho^2$  are neglected. The symplecticity (6) is exactly obeyed.

### 3.1.2 Tracking simulations

As seen in the previous section, a realistic description of the accelerator structure, fully adequate to compute single-particle trajectories, is difficult, if not impossible. Approximations must be tailored to the specific problem under investigation. Simplifications are also imposed by limitations in computing power.

Simulations with thin-lens approximation and symplectic integrators of the equation of motion, like Eq. (61), are considered as the master tool for quantitative estimates of particle behaviour in large accelerators like the LHC, since the length of individual magnets is small compared with the accelerator radius. They provide symplectic solutions for a dynamical system that approximates sufficiently well the entire accelerator. A sequence of linear transfer matrices interleaved with localized polynomial non-linearities should be computed. Reliable results are easily obtained since computer rounding errors can be kept under control [14]. However, vast computing power is required to get reliable estimates of the dynamic aperture as a function of various lattice and beam parameters. The thin-lens description is usually extended to guiding and focusing fields and, in general, does not imply relevant changes to orbit functions.

There are several computer codes by which large accelerators can be described. In the case of the LHC, two of them are routinely used for numerical simulations: MAD [15], developed at CERN, and SIXTRACK [16], developed at DESY. Both of them have scalar versions to be processed in the modern farms of workstations as well as vectorized versions to make use of modern parallel processors.

### 3.1.3 Maps

The use of non-linear maps in single-particle beam dynamics has been intensively investigated in the last fifteen years. It is outside the scope of this paper to present this activity in an exhaustive manner. Excellent review articles are available, like those in Refs. [17,18]. Here we shall limit ourselves to describing those concepts that have been applied in the design of the LHC.

In linear lattices, particle coordinates can be propagated along the accelerator azimuth by Twiss transfer matrices. The use of maps can be extended to non-linear dynamics with some precautions. This extension, originally motivated by the need to speed-up long-term tracking simulations in hadron colliders, in fact provides a powerful tool for handling dynamical quantities, like the tune dependence with the amplitude and the momentum, the distortion functions and the smear, the higher-order non-linear invariants, and finally the Fourier harmonic coefficients of the resonance driving terms. Non-linear matrices can be constructed very efficiently with differential algebra techniques using Taylor expansion to some higher order of algebraic operators [19]. One-turn Taylor maps resulting from the composition of all the linear and non-linear elements in the accelerator are inherently not symplectic because of the higher-order truncation, therefore inappropriate to preserve the volume in phase space. One of the ways to restore symplecticity is to replace the truncated map with a normal form [20–23], that is an integrable map, represented by a rotation of an angle depending on the amplitude of the orbit. Mathematically this operation implies the neglect of the non-integrable part of the map and the finding of a polynomial transformation of coordinates that conjugate the original map to a simpler and more symmetric map, which has explicit invariants, and explicit iteration formulae. The conjugation equation of a given map with its normal form is formally the same as the similarity transformation that brings a matrix to its diagonal form:

$$\Phi(\zeta)^{-1} \mathbf{M}(Z_c) \Phi(\zeta) = U(\zeta) . \quad (62)$$

Courant–Snyder coordinates for  $\mathbf{M}$  are complex, i.e.  $Z_c = (x - ip_x, x + ip_x, y - ip_y, y + ip_y)$ , in the case of 2-D degrees of freedom. The new coordinates are  $\zeta = (\zeta_1, \zeta_1^*, \zeta_2, \zeta_2^*)$ .

The transformation from the new to the old coordinates is tangent to the identity, since:

$$Z_c = \Phi(\zeta) = \zeta + \sum_{i \geq 2} \Phi_i(\zeta) , \quad (63)$$

where  $\Phi_i(\zeta)$  are homogeneous polynomials of order  $i$  in the new coordinates  $\zeta$ .

The normalized map  $U(\zeta)$  contains the same linear part  $\Lambda$  of  $\mathbf{M}$ , and can be expressed as a polynomial expansion:

$$U(\zeta) = \Lambda \zeta + \sum_{i \geq 2} U_i(\zeta) , \quad (64)$$

where  $U_i(\zeta)$  are polynomials of order  $i$  that obey special symmetry rules [23].

Formally, one can always build a normal form  $U$  of a non-linear map  $\mathbf{M}$ . However,  $\Phi$  and  $U$  are in general divergent in any open neighbourhood of the origin, because of the non-existence of an analytic invariant of motion for the original map. In spite of this, normal forms truncated at an order  $m$  can be used to interpolate the orbits of  $\mathbf{M}$  in judiciously chosen domains. The truncation, in general, implies that the symplectic conditions are obeyed up to an order  $m$  in the new coordinates. On the other hand, the truncated normalized map has an optimized order of accuracy. Above it, the approximation is improved at lower amplitude and worsened at higher amplitude. The domain of convergence is limited by resonances of low order that are allowed by the truncated Taylor map. There are ways to handle the first limiting resonance, with resonant normal forms [24], which have not yet been made of practical use.

In the LHC, the mapping approach based on Taylor expansion and normal form is used to evaluate the dependence of tune-shift on the amplitude and the momentum due to systematic field-shape imperfections [25]. In this way it is possible to identify the multipoles that are more dangerous for the stability of the motion, taking into account the quite strong higher-order cross terms, and to define and optimize the most suitable scheme of multipolar correctors.

Higher-order Taylor maps are also used to estimate the dynamic aperture in a faster way than with the usual element-by-element tracking [26]: however, in the LHC, this approach is non-controversial only for simulations up to few  $10^4$  turns. By increasing the order of the map, the violation of area-preserving transport can be made arbitrarily small, but the map size grows exponentially and the computing speed decreases accordingly. An interesting result is that one can correlate the accuracy of the truncated Taylor map tracking to the size of the high-order terms in the map. Alternatively, one can restore the symplecticity of the Taylor map by a linear scaling transformation to the particle coordinates at each turn [26].

### 3.1.4 Early indicators of chaos

Early indicators of chaotic motion have been used to speed up the estimate of the dynamic aperture in several accelerators and colliders, and, in particular, in the LHC. The exponential divergence of two initially very close trajectories is a criterion for chaos, a linear growth indicating regular motion. The exponential coefficient, called Lyapunov exponent [27], can be used to localize stochastic layers in the phase space and eventually to identify the stability border below which its value is zero.

Rigorously speaking, the maximal Lyapunov exponent is defined as:

$$\lambda = \lim_{d(0) \rightarrow 0, t \rightarrow \infty} \frac{1}{t} \log \left| \frac{d(t)}{d(0)} \right| \quad \text{with} \quad d(t) = \left\| \vec{d}_1(t) - \vec{d}_2(t) \right\| , \quad (65)$$

where  $\vec{d}_1(t)$ ,  $\vec{d}_2(t)$  are the phase space coordinates of two particles initially very close to each other. The routine way to evaluate it is to track simultaneously two particles with a slightly different initial amplitude, and to compute periodically and plot their mutual distance  $d$  in the phase space. A schematic illustration of the regular and chaotic evolution of  $d$  with time is shown in Fig. 6.

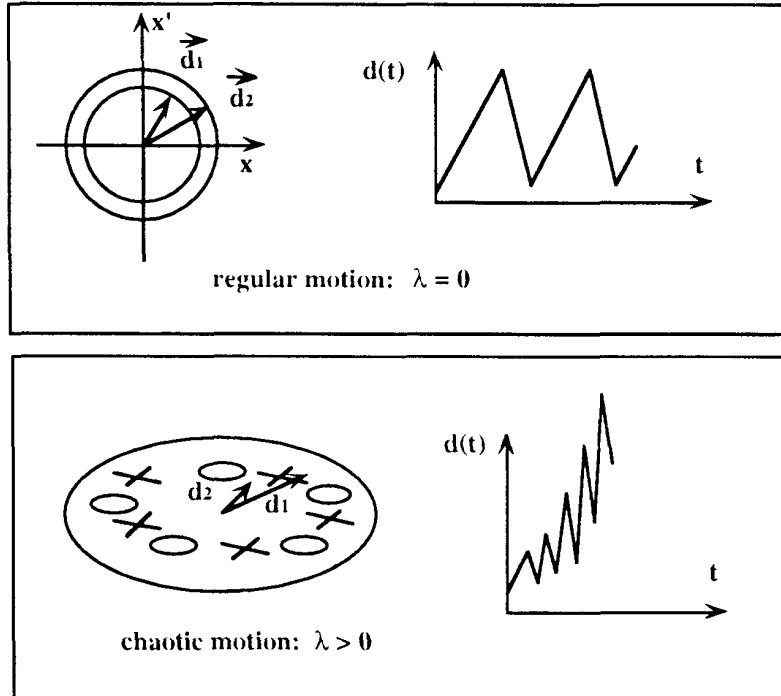


Fig. 6: Graphic method to evaluate the Lyapunov coefficient. The distance  $d$  of two initially very close particles is plotted as a function of time.

An equivalent method, better adapted to non-linear maps  $\mathbf{M}$ , is based on the analytical evaluation of the Jacobian  $M$  in the phase-space domain of interest. The eigenvalues of  $M^k$  evolve exponentially if the motion is chaotic:

$$\lambda = \lim_{k \rightarrow \infty} \frac{1}{k} \log (\text{max. eigenvalue of } M^k) . \quad (66)$$

The predictability of the two methods is enhanced when the non-linear deformation of the phase space is removed by a normal forms type change of coordinates [28].

It is currently admitted that through early indicators of chaos a conservative estimate of the dynamic aperture can be obtained with less computing power than for standard element-by-element tracking.

### 3.1.5 Figure of merit and data processing

The ‘linear aperture’, based on smear and tune-shift with the amplitude, was widely used in the past [29] to estimate non-linear effects, since threshold values for detuning and amplitude distortion were considered sufficient to ensure long-term stability. However, the validity of this extrapolation has not been confirmed by more profound studies. Therefore, intensive tracking and sophisticated data-processing are preferred nowadays to estimate the dynamic aperture, after a preliminary selection of rather few significant cases, on the basis of short-term simulations [30]. Results are presented in the graphical form of ‘survival plots’ that depict the maximum number of stable turns as a function of starting amplitude [31]. Survival plots and early indicators of chaos provide a practical estimate of the stable region.

Dense survival plots are ragged and show a large spread in the survival time close to the chaotic border, rapidly decreasing at larger amplitudes, as shown in Fig. 7. Such an irregular shape reflects the local origin of the particle instability: at moderate amplitude in presence of weaker perturbations, the escape time is largely influenced by microscopic changes of initial coordinates; at large amplitude, instead there are only fast losses.

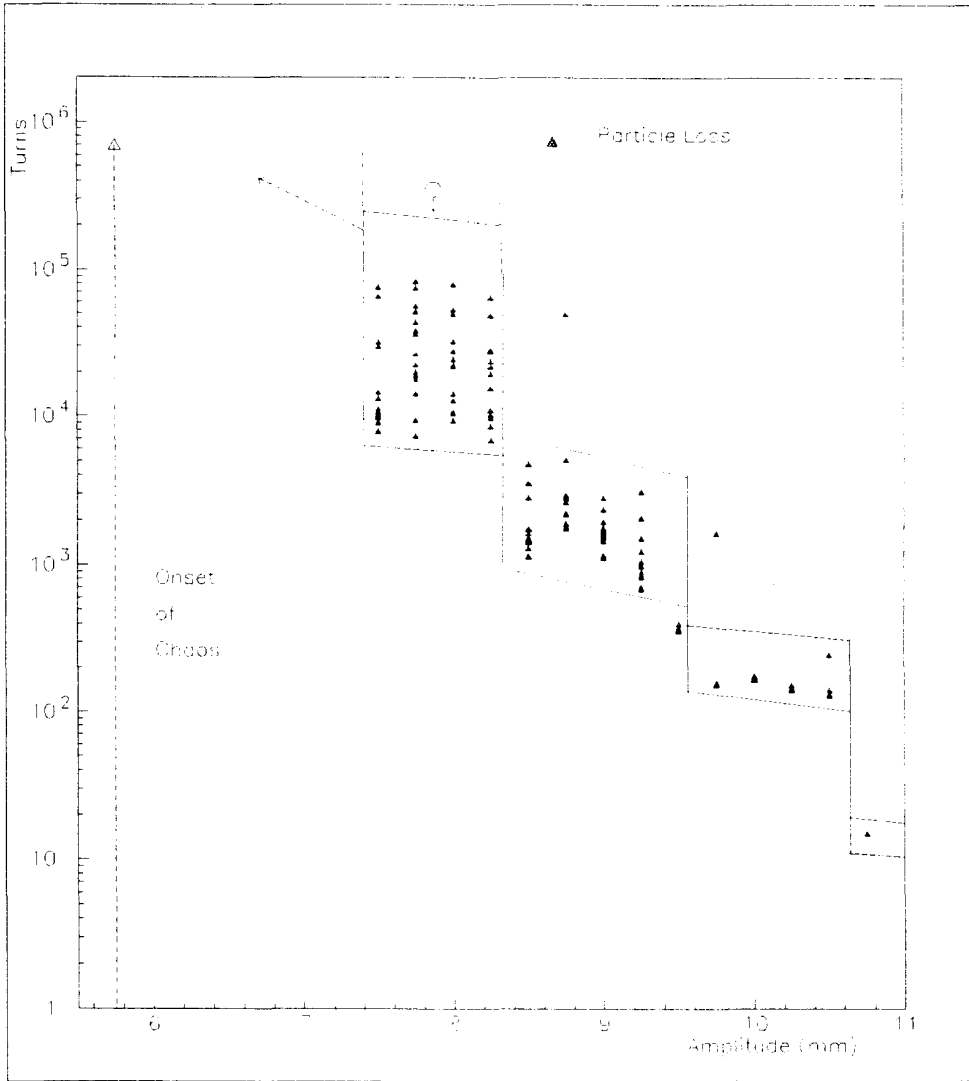


Fig. 7: Dense survival plot.

Under the influence of non-linearities, particles migrate across different nets of resonances. This phenomenon is presented in Fig. 8, where the turns are plotted in the working diagram as a function of time, for two initially nearby particles undergoing chaotic motion.

In the vicinity of the long-term dynamic aperture, the loss mechanism is in general sudden: the particle may stay confined even for millions of turns and then diverge in a few thousand turns.

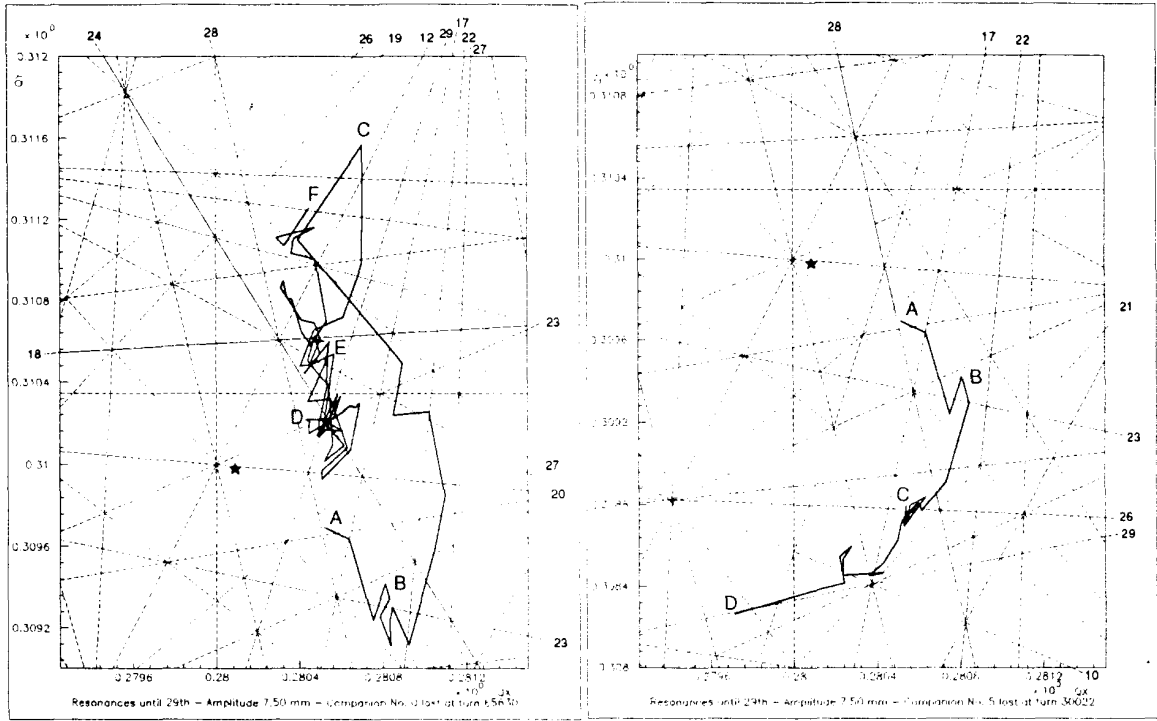


Fig. 8: Evolution of tunes with time of two initially close particles undergoing chaotic motion.

### 3.2 Applications to accelerator design

Hadron colliders, like the LHC, must operate with negligible loss for long periods, up to  $10^8$  turns, in spite of the unavoidable field shape imperfections. An upper limit to unintentional multipoles and practical compensation strategies have to be devised for a safe operation. This implies a thorough understanding of the influence of the non-linearities on the long-term behaviour of particle trajectories. Analytical methods available are not yet fully exploited. Numerical simulations are too cumbersome and time-consuming for an exhaustive overview of all the possible situations. Nevertheless, remarkable progress has been made through heuristic approaches proposed in the recent past, based on the investigation of simplified non-linear models of the lattice and on the use of empirical criteria for beam stability.

Too crude simplifications of the lattice structure itself have dramatic effects on non-linear performances. Cell lattice models with only regular cells and no interaction regions show a regular azimuthal pattern of the orbit functions and in particular of the betatronic phase advance leading to unrealistic enhancement of the particle stability. They are in general used for numerical studies of simple dynamical systems such as the Hénon or higher-order maps. A more realistic way to drop the insertions is to replace them with equivalent rotation matrices. Part of the chromatic aberration and some unintentional field errors are disregarded in this way. In addition, this technique makes it particularly difficult, if not impossible, to track in a correct manner off-momentum particles performing synchrotron oscillations. However relevant information can be gained with less computing power and complexity, especially during the injection plateau, where the stability of motion is mainly determined by non-linear perturbations in the arcs of regular cells. This approach was used, for instance, to determine the optimum value for the length and the phase advance of the LHC cell [32], fixed to about 100 m and 90°, respectively. More advanced studies are generally based on models with realistic descriptions of the insertions.

The field-shape imperfections are equivalent to multipoles up to large order, which can be expressed as the sum of two parts, one systematic and the other random. The general agreement, based on the magnetic measurements of the Tevatron and Hera [33], is to stop at order 11 in the multipolar expansion and to neglect correlation between random multipoles of

different orders. Systematic errors are larger at injection due to persistent currents. Large low-order systematic multipoles, like  $b_3, b_4, b_5$  in superconducting dipoles, or  $b_6$  in superconducting quadrupoles, provoke a sizeable detuning with the amplitude and the momentum, which can be corrected either locally [34], as in the LHC lattice version 2, or using a clever cancellation of the detuning terms by means of Simpson rules [35], as in the LHC lattice version 1. In the latter case, multipolar correctors are to be located near the main quadrupoles as well as at about the middle of each half-cell [25]. Octupolar imperfections can be treated in a global manner. For instance, they have, in the LHC, a particular behaviour related to the symmetry of the magnetic field in two-in-one magnets: the integrated value along the azimuth is expected to be zero, therefore the detuning with the amplitude is expected to be self-compensated without specific correctors. Large higher-order systematic multipoles, like  $b_7$  and  $b_9$ , destabilize off-momentum particles and have to be minimized by design: tolerable values for the LHC have been found to be of the order of  $2 \times 10^{-6}$  and  $5 \times 10^{-7}$  units at 1 cm radius, respectively.

Random imperfections, which vary from magnet to magnet owing to manufacturing tolerances, are the main source of non-linear resonances and distortion functions. Statistical distributions can easily be predicted, but are insufficient for a complete knowledge of the non-linear optics, since resonance strengths depend on the specific sequence of the random errors around the ring rather than on statistical properties. Therefore, criteria for magnet design are to be studied on several non-linear lattices, with different sequences of random multipoles. In fact, there are many parameters that limit the stability of the particle motion in hadron colliders, therefore the first task is to identify the most important ones, in order to reduce to a reasonable amount the enormous computing time required for an exhaustive set of simulations.

Heuristic approaches are in general applied, like in the design of the LHC, briefly described hereafter. Parameters routinely considered in the accelerator models are residual closed orbit, linear coupling due to imperfections, synchrotron motion, and residual ripple in main power supplies. Chromaticity and non-linear detuning are corrected with a proper set of correctors. Special cases with some residual uncompensated chromaticity are considered as well. Short-term dynamic aperture is first evaluated by tracking particles of different starting amplitudes for  $10^3$  turns. This is fast and well-suited for a first exploration of the space parameters, and is also sufficient to reveal the most important features of the non-linear phase space. Ten different seeds are used to fix the test samples of the random errors. Appropriate subsets of them are considered to disentangle the effects of the dipole imperfections from those of the quadrupole imperfections in a machine with a perfect closed orbit and no linear coupling. By choosing three representative seeds in each distribution, i.e. one with the smallest, one with the largest, and one with an average value of the aperture, one can easily check the combined effect of the dipole and the quadrupole errors and identify a limited number of representative sets of non-linear lattice models to be investigated with long-term tracking simulations. With this strategy [30], beam stability has been found to be strongly influenced by linear lattice parameters like tune, residual linear coupling, and peak  $\beta$ -values in the insertion quadrupoles as well as by a residual chromaticity of a few units. Instead, residual closed orbit associated with magnet misalignment and tune ripple of a few  $10^{-4}$  units showed a weak interference with beam stability. Particles above the stable region are expected to diffuse towards the vacuum pipe at a speed strongly increasing with the transverse amplitude. A set of collimators [36] is used to absorb them before they hit the magnets and provoke an unwanted deposition of energy in the superconducting coils. The transverse position of the primary collimator defines the mechanical aperture of the accelerator. It is basically fixed taking into account the mechanical tolerances of the cold bore and of the thermal beam screen in the main magnets, the expected peak-values of the closed orbit, of the dispersion, and of the  $\beta$ -function modulation, and, of course, the optimum value of the separation between the primary and the secondary collimators. For a safe operation, careful matching of physical aperture and stability border is to be performed [30]. With a small mechanical aperture, only trajectories with small amplitude oscillations are allowed, which are weakly perturbed even in presence of large field-shape imperfections, whilst, with larger mechanical apertures, and larger amplitude oscillations, the non-linear perturbation becomes larger and the size of the magnetic errors start to play a leading role for the dynamic aperture. On the other hand, we believe that particles with amplitudes up to the chaotic boundary are stable, although the non-linear perturbations induce a finite smear of their

trajectories, whilst particles with larger amplitudes may become unstable after a sufficiently large number of turns. Ideally, the chaotic limit should be equal to the dynamic aperture evaluated in the presence of collimators, in which case only the unstable particles will be intercepted by the collimators. In this respect the mechanical size and the field quality of the LHC at injection have been found to be well matched to a value of  $6\sigma$ , i.e. of 7.2 mm, which is considered a wise choice for the needed dynamic and physical aperture.

Strategies of magnet sorting have been invented, by which the magnets are installed in such a sequence in the machines as to minimize the combined non-linear effects. For practical and theoretical reasons, the sorting scheme should be as local as possible and must refer to a limited kind of multipoles. Different solutions have been proposed [37–39]. By introducing a quasi-periodicity of multipoles every two betatron wavelengths, the harmonic content of non-linearities can be shifted away from harmful frequencies. Alternatively, small groups of magnets, typically ten, are ordered in such a way as to minimize a broad band of non-linear driving terms computed to 2<sup>nd</sup> perturbative order, contributing to resonances up to order 6. The first method is used in the LHC and the SSC, the last method is used for HERA and is still under investigation for the LHC.

#### 4. REVIEW OF DEDICATED EXPERIMENTS

Since 1986 dedicated experiments have been performed in the CERN SPS and in the FNAL Tevatron to study the beam dynamics in the presence of strong non-linear fields intentionally introduced along the accelerator circumference. The motivation is to study the refinement of aperture and field quality criteria for the design of future large hadron accelerators like the LHC, SSC, or RHIC.

The experimental procedure consists in exciting already existing sextupoles in order to introduce non-linearities in a controlled fashion in an otherwise linear lattice. To probe large amplitudes, either a pencil beam with small emittance and momentum spread is used, to which a large enough coherent deflection is applied, or a large emittance beam is created with repetitive small-amplitude coherent kicks. In the first case, a few hundred turns are sufficient to create a ‘hollow’ distribution of charges around the central orbit due to non-linear filamentation, in the second case, a few kicks are required to spread out the particles all around the available physical aperture of the accelerator. The proton behaviour is observed with several instruments: current transformers record lifetime, Schottky noise detectors give tune and tune-spread, flying wires provide transverse profile, and orthogonal pairs of position monitors are able to produce a phase-space portrait. Sinusoidal tune modulations are added to simulate the effect on the beam stability of the unavoidable ripples in power supplies.

Interesting experiments have been started more recently at the IUCF cyclotron facility in Indiana University, with the specific purpose of exploring non-linear particle motion, in particular along the resonant islands [40–43]. Only the necessity to be concise forces us to drop their description and to concentrate our attention on the experiments at CERN and FNAL.

##### 4.1 Experimental conditions

Well-understood and clear experimental conditions, with most of the spurious effect eliminated and the phenomena under study carefully isolated, are required to make meaningful comparisons between the experimental results and the numerical simulations of them with computer tracking programs.

In the SPS, low-intensity beams of  $10^{11}$  to  $2 \times 10^{12}$  protons undergo linear motion between 100 GeV/c and 250 GeV/c, since the remanent fields effects can be neglected, as are the space charge effects, whilst the saturation effects in the magnets are not yet perceptible. An energy of 120 GeV/c is finally selected for dynamic aperture studies, so as to benefit from the maximum strength of the added non-linear fields. In the Tevatron, intensities of  $10^{10}$  particles are used, and an operational energy of 150 GeV/c is chosen for similar reasons.

Intentional non-linearities are provided by powering independently several sextupoles foreseen for the resonant extraction of the beam at top-energy. Eight sextupoles evenly placed

along the ring are routinely used in the SPS, sixteen sextupoles are used in the Tevatron. Positive and negative values of the current are alternated around the rings in such a way as to suppress the third-integer resonances, except in early experiments where that resonance was strongly excited. The chromaticities are corrected using four families of sextupoles in order to obtain an almost flat pattern of the tunes as functions of the momentum deviation.

Closed-orbit deviations and linear coupling are in general well compensated: a residual r.m.s. orbit not in excess of 0.5 mm and a minimum horizontal–vertical tune approach of the order of 0.002 units are currently imposed.

Except for occasional situations, a beam with one single bunch is used in the Tevatron, whilst a debunched beam is used in the SPS.

## 4.2 Results in the CERN-SPS

### 4.2.1 Short-term dynamic aperture experiment

Studies of the short-term dynamic aperture were started in 1986 while the SPS was operating in fixed target mode [44,45]. The beam was injected at  $14 \text{ GeV}/c$ , accelerated up to  $120 \text{ GeV}/c$  and allowed to circulate at this energy for eight seconds on a magnetic flat top. The full ring was filled with bunches and the RF was kept on. At the beginning of the  $120 \text{ GeV}/c$  flat top the intentional sextupoles were energized and the beam emittance increased until losses occurred. This was done by repeatedly deflecting the beam with the fast kicker normally used to measure the tunes. In the absence of intentional non-linearities, it was sufficient to pulse the kicker twice at its maximum deflection to reach the machine aperture in the vertical plane, which was of the order of  $\pm 15 \text{ mm}$ . In these conditions the intensity losses are abrupt in time. When the sextupoles were energized, the acceptance was reduced. The amplitude of the two kicks was therefore lowered so as to produce losses not in excess of 10–20% of the circulating intensity, these losses started just after the second kick and lasted for a few seconds. Following that, in all cases there was another period of a few seconds before the end of the flat top with no visible losses. The size of the surviving beam measured with a high gain of the wire scanner was assumed to be the dynamic aperture of the machine. This mode of operation is schematically illustrated in Fig. 9.

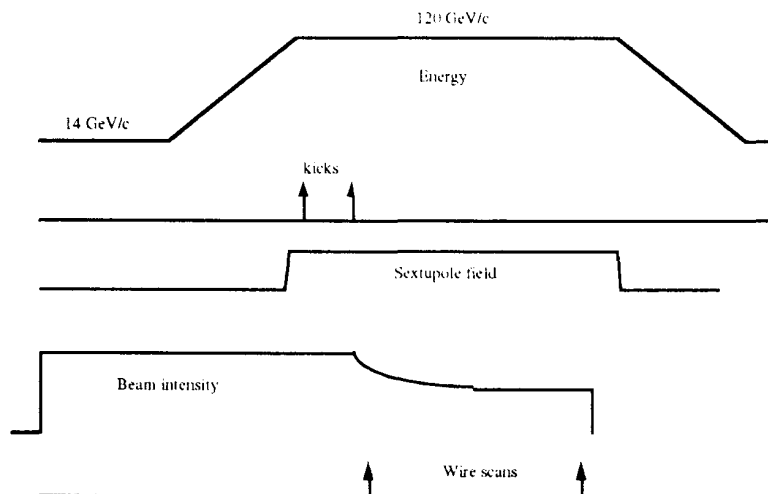


Fig. 9: Mode of operation of the CERN-SPS during the short-term dynamic aperture experiment.

The experiment was performed first with intentional sextupoles exciting the third-integer resonance and later without exciting it. In the latter configuration, several working points around the fifth-order resonances were explored for which a horizontal dynamic aperture of 13–21 mm was measured. Once the synchrotron motion and closed-orbit distortions were taken into account, computer tracking simulations performed over up to  $10^5$  turns, i.e. a few seconds of real machine time, were able to provide estimates of the dynamic aperture in reasonable agreement with the measured value. The loss mechanism was clearly related to the crossing of

the fifth-order resonances, and the upper limit of the detuning and the smear of stable trajectories were found to be of the order of 0.01 units and 0.035 respectively.

In 1988, another experimental session was devoted to the study of the short-term stability, with the same machine conditions as in 1986. At that time, an instrument was made available to record the beam oscillation over several thousands of turns in consecutive position monitors separated by about  $\pi/2$  in betatron phase. Using this instrument, phase portraits could be drawn and tunes could be precisely measured both in pulsed and in storage mode [46].

To explore the effect of the intentional non-linearities, a pencil beam of 1.3 mm r.m.s. size was used, which was obtained by bringing the larger injected beam in proximity with a collimator. Horizontal hollow beams of amplitudes as large as the vacuum chamber could be produced by firing the fast kicker once. Two working points were explored, one near to the fifth- and the other near to the seventh-order resonances. The detuning was measured as a function of the oscillation amplitude, proportional to the kick voltage, and found to be in a very good agreement with the numerical simulations by tracking. The dynamic aperture was measured by adding the amplitude of the coherent oscillation to twice the r.m.s. beam size for which losses were just visible. For comparison, the boundary of the chaotic motion region was computed by numerical simulations with the program SIXTRACK [16]. The agreement between experimental data and simulations was excellent, as for instance for the working point near the fifth-order resonances: the measured aperture was between 15.8 mm and 20.2 mm, the numerical estimate of the chaotic border was 17.6 mm.

With the previous experiments the concept of short-term dynamic aperture was clarified to a large extent. In the presence of strong non-linearities, particles can be lost in a few hundred turns by the effect of higher-order resonance crossing due to the detuning. In these conditions, the Lyapunov coefficient, easily obtainable by numerical simulations, is a good predictive indicator of the chaoticness of the trajectories and of the instability of the motion.

In 1989, the non-linear detuning and its compensation were studied and their effect on dynamic aperture was carefully explored. The measurement of the amplitude-dependent tune shift was again found to be in good agreement with tracking. Figure 10 shows the experimental data of 1989, very close to that of 1988. Moreover, Fig. 10 shows clearly how strongly the particle losses can be influenced by the use of octupoles. By adequately powering them in the SPS we succeeded in reducing the non-linear detuning by roughly an order of magnitude, which at the same time improved the dynamic aperture by 30%. This result suggests that the correction of the non-linear tune-shift in superconducting hadron colliders can be an appropriate method to improve the performance of these very non-linear machines and in particular to reduce short-term losses.

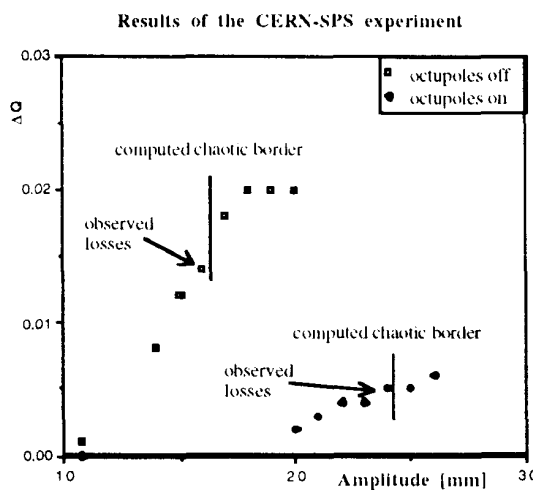


Fig. 10: Compensation of the detuning with the amplitude by means of octupoles.

#### 4.2.2 Sextupole-induced diffusion

An early experiment at the Sp $\bar{p}$ S, showed that circulating particles have a transverse diffusive behaviour in the presence of localized beam-beam collisions, due to non-linear resonances, tune-spread, and noise. In the context of the studies for the design of large superconducting hadron colliders, an important issue is whether the unavoidable non-linearities in the guide fields are likely to create a diffusion mechanism similar to that induced by beam-beam interactions, since both kinds of non-linearities create tune-spread and resonance excitation, even if in the two cases the dependence with particle amplitude is quite different. This issue was addressed in 1988 at the SPS, with a dedicated experiment on diffusion induced by sextupoles [45].

A debunched beam was stored at 120 GeV/c, and the horizontal beam emittance was slowly increased by repeatedly firing a kicker, until a few per cent losses were noticed. The eight sextupoles were powered so as to avoid excitation of the third-order resonance. The beam intensity was recorded, while certain actions were performed, in order to bring evidence for proton diffusion. An horizontal scraper was introduced close to the edge of the beam in order to clear the tails of the transverse particle distribution. In doing this, a small fraction, typically about 1%, of the circulating particles was lost abruptly. Subsequently, an exponential decay of the intensity was measured. The scraper was then retracted by a few millimetres, typically 2 mm. Consequently, the intensity remained constant for the time required for the particles to fill the gap between the innermost and the retracted position of the scrapers. The time duration with flat intensity could be used to evaluate the average value of the diffusion coefficient. The plateau regime was followed by another period with exponential decay of the intensity, the time constant of which was slightly larger than the initial one. When the scraper was moved back to the innermost position, another abrupt loss of beam was visible, followed by an exponential decay with the same time constant initially observed. We see here a clear signature of a ‘diffusion process’.

With the working point near the fifth-order resonances, a diffusion rate of 3 mm/min was measured at an amplitude of 12.6 mm, and 6 mm/min at 15.4 mm. At 18.1 mm the diffusion was so fast that it could not be measured with the procedure described above: this is just across the short-term dynamic aperture sitting between 15.8 mm and 20.2 mm.

Similar measurements were done at working points near to the seventh-order resonances. In this case the largest amplitude at which no significant diffusion could be detected was of 9.2 mm.

The measurement was repeated in the absence of the added sextupoles. There was no sign of diffusion up to an amplitude of 22 mm, well outside the dynamic aperture measured in the previous experiment.

Numerical simulations performed for up to  $10^6$  turns did not reveal any chaotic motion inside the short-term dynamic aperture. This changed dramatically when a tune modulation of  $3 \times 10^{-3}$  units was introduced in the tracking to take into account the realistic situation of the main power supplies, optimized at that time for the operation in fixed-target mode. This is to be expected from the application of the Chirikov criterion for overlap of satellite resonances. The value of the Lyapunov coefficient computed with tracking now decreased as the particle amplitude was reduced, and from this, lower and lower diffusion rates could be expected, in qualitative agreement with the experimental results.

With a view to evaluating the predictive power of the detuning and the smear as indicators of stable motion, Fig. 11 was drawn which included all the experimental situations considered in 1986 and 1988. The rectangular box represents the criteria used in 1988 for acceptance of the LHC lattice: it was supposed that in this rectangle the machine would be sufficiently linear to assure a good, comfortable operation. It appeared clearly from the experimental data that the LHC criteria were sufficiently conservative as far as the short-term dynamic aperture was concerned, however, they were certainly insufficient to ensure a good lifetime in storage mode, owing to the magnetic-imperfection-induced diffusion.

### Short-term stability: criteria for $\Delta Q$ and smear

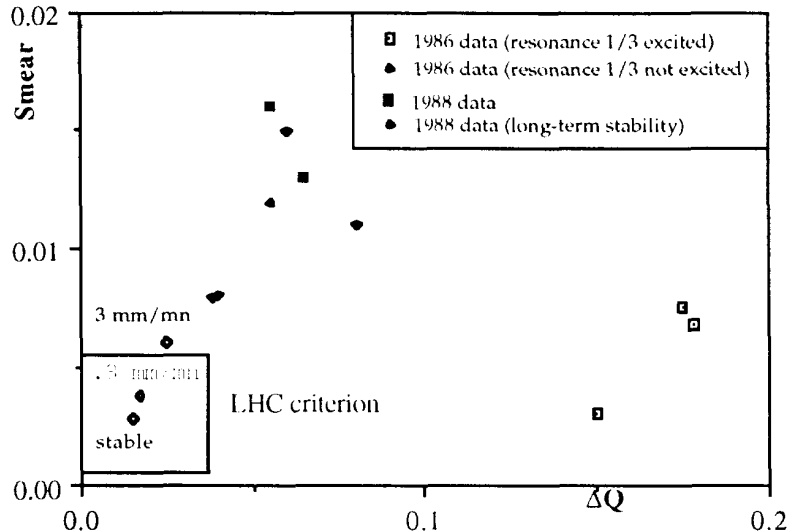


Fig. 11: Predictive power of detuning and smear as indicators of stable motion.

#### 4.2.3 Effects of an external modulation of the tune

Experiments were performed at the SPS in 1989, 1990 and 1991 to get quantitative estimates about the influence of sinusoidal modulations of the tunes on the dynamic aperture [47,48].

As a preliminary step, the time structure and the spectral characteristics of the ripple inherent in the main power supplies were measured in different operational conditions, using the Schottky noise detector for continuous-tune measurements [49]. At a 120 GeV/c energy plateau, with the power supply settings appropriate for pulsed operation, the tune variation with time was of the order of  $\pm 10^{-3}$  units. The variation was reduced to about  $\pm 2 \times 10^{-4}$  units, when the main power supply control was improved as for collider operation. In both cases, the power spectra of the ripple showed a dominant peak at a frequency of 50 Hz, with additional peaks of decreasing power at the higher harmonics of 50 Hz, extending up to 1 kHz.

The effect of the induced tune modulation was studied on a low-emittance debunched beam stored at 120 GeV/c. All the circulating particles were deflected horizontally at large amplitude in a ‘hollow’ beam, by firing a kicker once. The eight sextupoles were powered so as to avoid excitation of the third-order resonance, while provoking non-linear motion. A sinusoidal excitation of the tunes was induced by powering a special quadrupole, located near a focusing main quadrupole. The amplitude of this artificial, controlled ripple can be increased well beyond that of the natural ripple of the main power supplies. Modulation depths up to about  $\pm 2 \times 10^{-3}$  tune units could be explored, in a frequency range limited to about 600 Hz by the inductance of the quadrupole. The beam stability was studied with the scraper retraction technique, described in the previous section. The experimental layout is schematically illustrated in Fig. 12.

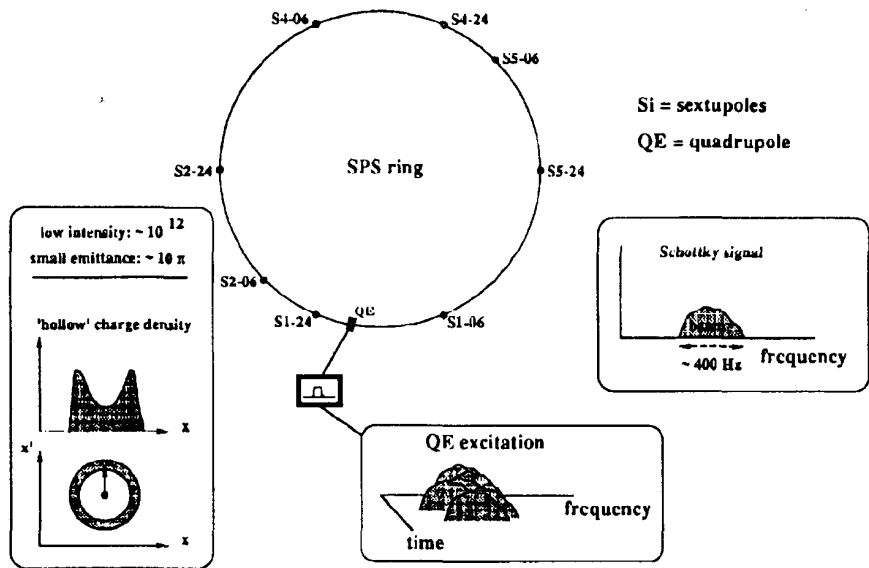


Fig. 12: Mode of operation of the CERN-SPS during the long-term dynamic aperture experiment.

During the experiments, care was taken to compensate for the closed-orbit distortions and the linear coupling. The tune was chosen very carefully so as to minimize the effect of resonances. Octupoles were used to decrease the amplitude-dependent tune shift so as to better locate the working point in between the most dangerous resonances. Even if the particles were initially displaced in the horizontal direction, the net of resonances explored by the beam, in general, provoked horizontal–vertical non-linear coupling, with consequent beam losses in both planes. Therefore, to measure the diffusion speed with the retraction method, both horizontal and vertical scrapings were required.

In storage-mode experiments in 1989 and 1990, the beam size was increased by a single large-amplitude coherent kick. The tune, after applying the kick, was adjusted so as to stay away from the fifth- and seventh-order resonances:  $Q_H$  between 0.623 and 0.640,  $Q_V$  between 0.529 and 0.540. Measurements with no tune modulations and with modulations of 9 Hz, 40 Hz, and 180 Hz and the same depth of  $\pm 8.0 \times 10^{-4}$  tune units were performed. As the scrapers were retracted from the peripheral of the beam, there was the usual period of no noticeable losses. When the first scraper was reached by particles, a drop in lifetime appeared, followed by a second drop when the second scraper was also reached. This is indeed what we can see schematically in Fig. 13. Diffusion speeds of about 0.5 mm/min were recorded without tune modulation and of about 2.5 to 5 mm/min with tune modulation. The diffusion process, however, was almost independent of the modulation frequency.

The importance of the modulation depth was pointed out in a similar experiment performed in 1991. By varying from  $1.1 \times 10^{-3}$  to  $2.2 \times 10^{-3}$  the amplitude of the sinusoidal modulation, an increase of the diffusion speed by a factor of ten was observed for each modulation frequency.

In comparison with the effect of a monochromatic beam excitation, combining two different frequencies in the tune modulation was expected to lead to a sizeable reduction of the dynamic aperture. This effect was tested in the 1991 experiment. Initially there is no ripple and no measurable diffusion. With a tune modulation of  $1.65 \times 10^{-3}$  amplitude and 9 Hz frequency, the beam lifetime drops to seven hours. The losses stop immediately when the ripple is switched off again. Two combined sinusoidal modulations of  $0.8 \times 10^{-3}$  amplitude each and of 9 Hz and 180 Hz frequency, respectively, produce a severe drop of the lifetime to two hours. In the two situations the same total modulation amplitude was used, however, the

effect on beam stability is dramatically larger with two frequencies than with only one frequency. The qualitative explanation of that invokes the Chirikov criterion: with two frequencies, primary resonances have richer spectra of sidebands and more effective overlap.

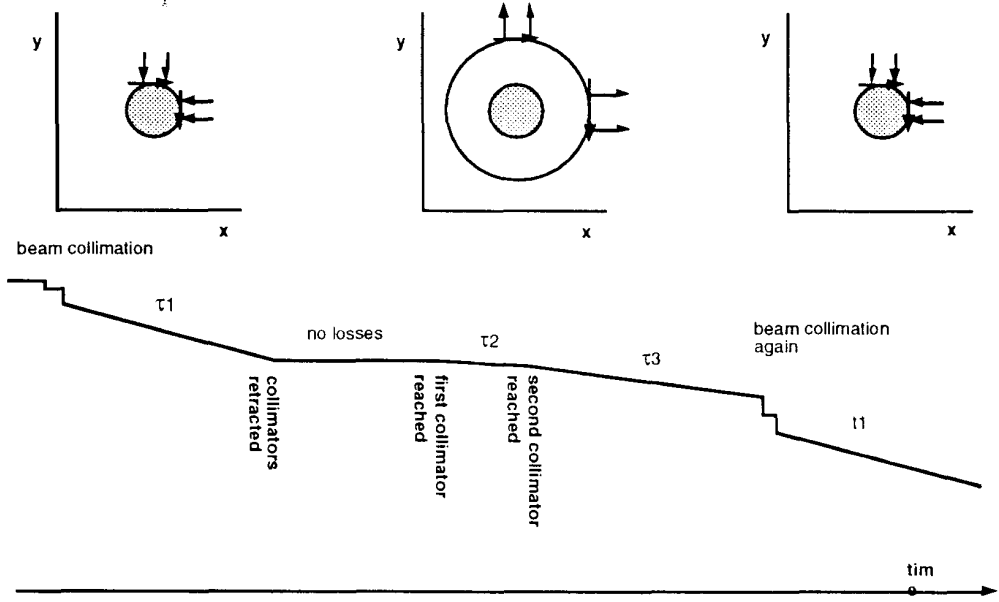


Fig. 13: Illustration of the scraping retraction technique to measure the diffusion coefficient.

From the results discussed above it is clear that in a collider with large non-linear field-shape imperfections, the total ripple amplitude which can be tolerated in the main power supplies is a crucial issue. The present understanding is that tune modulations larger than those observed in the SPS in collider mode, i.e. a few  $10^{-4}$  units, can be quite harmful for beam stability.

#### 4.2.4 Conclusive overview of the SPS experiment

The techniques for the experiment on diffusion and dynamic aperture at the CERN SPS are quite well mastered, although it requires a long and meticulous preparation to obtain clear machine conditions. However, its interpretation is far from being complete.

As far as short-term phenomena are concerned, the predictive power of the Lyapunov coefficient has been well assessed. It has also been proved that the detuning is a parameter strongly influencing the beam stability, therefore its compensation is considered beneficial for the design of future colliders.

Long-term effects are still not fully clarified. The diffusion mechanism itself is likely not to be governed by a simple Fokker–Planck equation. On the other hand, the diffusion process is inherently related to ripple, and empirical criteria are now available for the design of the power supplies of future colliders, which have to be stabilized in current to better than one part per  $10^5$ .

These kinds of studies are still continuing today, with both new experiments and numerical simulations in order to improve the quantitative understanding of the diffusion and the loss mechanisms. The hope is finally to find criteria for the field tolerances of the superconducting magnets for future colliders.

### 4.3 Results in the FNAL-Tevatron

#### 4.3.1 Tune-shift, smear and short-term dynamic aperture

Studies of the short-term dynamic aperture, non-linear detuning and smear, i.e. the r.m.s. fractional change in amplitude along phase space trajectories, were started in 1985 in the Tevatron [50, 51].

The beam, made of a single bunch of  $10^{10}$  protons, was stored at the injection energy, 150 GeV/c. The sixteen sextupoles were ramped up to the desired value of excitation in 10 s. After a further 10 s delay, a coherent betatron oscillation was induced by firing the Tevatron injection kicker. At each of several values of the horizontal tune, a number of kick amplitudes were employed, bounded from above by the onset of beam loss in the Tevatron without sextupoles. The principal data recorded at each condition were the turn-by-turn signals from two monitors, and the beam intensity. This variety of data was analysed to give smear and tune values to be compared with simulations. If the beam were a single particle, then the calculation of the smear from experimental data would reduce to a simple matter of minimizing a least square fit, using the lattice functions and the orbit positions at the monitors as minimization variables. The finite emittance and momentum spread of the beam add difficulties, since the non-linearity introduces a ‘decoherence’ of the centre-of-gravity motion. The ‘decoherence’ that arises from chromaticity can easily be corrected. But the dominant source of the ‘decoherence’ is the non-linear tune variation with the amplitude caused by the sextupoles. The calculation of the phase space distortion in the presence of this effect relies on a reconstruction of a single-particle motion by fitting a Gaussian distribution of the particles to the apparent amplitude reduction of the motion of the beam centroid. Tune dependence with the amplitude, smear and ‘decoherence’ damping time were measured with particular care at an horizontal tune around 19.4 units. Quantitative comparison between observed and calculated quantities showed an excellent agreement.

In a similar set of experiments, the horizontal emittance of the beam was slowly increased through the introduction of noise into the transverse damper, and the limiting emittance observed as a function of the sextupole excitation. Beam profiles were recorded throughout this process. The limiting beam size was taken to be a measure of the dynamic aperture, when less than the physical aperture, and compared with simulations. The measured aperture was approximately 20% less than the calculated aperture. This discrepancy was ascribed to effects affecting the loss observed over  $10^6$  turns, that were not included in the few  $10^2$  turns computer tracking simulations.

#### 4.3.2 Particle beam trapped in resonance islands

In creating ‘hollow’ beams at the Tevatron, it was observed that, for particular values of the kick amplitude and polarity, some fraction of the beam was trapped in resonance islands. The detection of such trapping turned out to be surprisingly easy, since, in the presence of ‘decoherence’ of the rest of the beam, the trapped particles continue to oscillate in a coherent fashion. In addition, both the phase-space plot and the spectral analysis of the transverse position signal as a function of time show that the sustained signal is associated with a fractional value of the tune. For instance at a tune near 19.4, the phase space plot typically showed five islands, whilst the Fourier analysis had power components peaked at two-fifths of the revolution frequency. External tune modulation was found to influence the lifetime of the persistent tune lines associated with particles trapped in islands. The interpretation of this phenomenon in terms of Hamiltonian theory is given in Ref. [52]. Comparisons with experimental data are reported in Refs. [51,53]. A concise description of the various arguments is presented here.

In a Poincaré plot ( $\theta, J$ ) representing the horizontal motion in the Tevatron, with a horizontal tune slightly below 19.4, protons launched at small amplitudes follow circular orbits. As the initial amplitude is increased, the tune increases with a parabolic law. Resonance islands appear at an appropriate amplitude, corresponding to rational tunes: five islands are visible as the tune approaches a value of  $2/5$  units. A proton launched inside one of the islands jumps two islands per accelerator turn, returning to its original island after five turns. Since the proton never escapes the island in the absence of external tune modulation, a resonant trajectory only visits a localized range of phase, that is the phase is locked and the tune is exactly  $2/5$  units.

Single-particle motion inside the island is represented by the five-turn Hamiltonian:

$$H_5 = 2\pi\left(Q_0 - \frac{2}{5}\right)J + \frac{1}{2}U(J)J^2 - V_5 J^{5/2} \cos(5\theta), \quad (67)$$

where  $U(J)$  parametrize the tune-shift with the action  $J$ , and  $V_5$  represents the strength of the resonance. The equations of motion are:

$$\begin{cases} \dot{\theta} = 2\pi(Q_0 - \frac{2}{5}) + UJ - \frac{2}{5}V_5J^{5/2}\cos(5\theta) \\ j = 5V_5J^{5/2}\sin(5\theta). \end{cases} \quad (68)$$

The motion of a proton inside one island is well approximated when Eqs. (68) are integrated over five turns. Protons infinitely close to the fixed point at the centre of the island are characterized by the resonant action  $J_R$ , and rotate at the island tune:

$$Q_I = \frac{5}{2\pi}(UV_5J_R^{5/2})^{1/2}. \quad (69)$$

Protons away from the centre rotate at a different speed owing to the non-linear detuning with the distance from the fixed point.

Phenomena that modify the distribution of particles inside the island have relaxation periods, until the new equilibrium distribution is reached, lasting of the order of  $1/Q_I$  turns.

Tune modulations of the type:

$$Q(t) = Q_0 + q\cos(2\pi Q_m t) \quad (70)$$

produce four distinct types of dynamical behaviour, in the control parameter space of tune modulation strength and tune ( $q, Q_m$ ).

For low values of  $q$  and  $Q_m$ , the tune modulation is slow and weak, so that  $Q(t)$  changes adiabatically. On account of this, the island amplitudes change slowly, but their phases are almost constant. This is the *amplitude modulation* regime.

As the tune modulation strength  $q$  increases at constant modulation time  $Q_m$ , the stable area of the islands shrinks, up to the point where there is no stable area at all and the adiabatic trapping is eventually lost. Close to the fifth-order resonance, the condition for adiabatic trapping is:

$$qQ_m < \frac{1}{5}Q_I^2. \quad (71)$$

When the relation (71) is violated the motion becomes *chaotic*.

A tune modulation, rapid but weak, causes the island fixed points to oscillate in phase but not in amplitude. Additional chains of modulational sideband islands appear around the fundamental tune of 2/5 units, spaced by multiples of the modulational frequency:

$$Q_{\text{sidebands}} = \frac{2}{5} \pm \frac{i}{5}Q_m \quad \text{with } i = 1, 2, \dots. \quad (72)$$

Phase averaging techniques, that are rigorous in the fast limit, show that the  $i^{\text{th}}$  sideband is negligibly small if the modulation strength  $q$  is smaller than the tune distance from the fundamental:

$$q < \frac{i}{5}Q_m. \quad (73)$$

This condition, with  $i = 1$ , is the boundary between *phase modulations*, when it holds, and *strong sidebands*, when it does not hold.

When sidebands are present, the Chirikov overlap criterion holds and *chaos* ensues if:

$$Q_m^{3/4}q^{1/4} < \frac{4}{(5\pi)^{1/4}}Q_I. \quad (74)$$

At the Tevatron, three of the five regions of the control parameter space ( $q, Q_m$ ) were made experimentally accessible.

In one experiment  $q$  and  $Q_m$  were linearly ramped for 1 s up to quite large values and then turned off. In another experiment, only  $Q_m$  was linearly ramped for 1 s, and  $q$  was taken constant and small. Tune modulation strength was varied in the range from few  $10^{-4}$  to  $10^{-3}$  units, with modulation frequencies up to 350 Hz. In this way, the boundary between amplitude modulation, phase modulation, and chaotic regions in  $(q, Q_m)$  space was explored, and found to be in a good agreement with analytical estimates.

Tune modulation strengths not larger than few  $10^{-4}$  units in a frequency range below few hundred Hz were suggested to be considered tolerable in the design of future colliders.

#### 4.3.3 Model for diffusion induced by sextupoles

In this experiment the Tevatron was used to study stochastic effects due to non-linear beam dynamics that cause ‘diffusive’ evolution of the beam distribution, even in the absence of external sources of noise [54]. Initially, ‘hollow’ beam distributions were created with  $10^{10}$  particles circulating in one bunch at  $150 \text{ GeV}/c$ . Then sixteen sextupoles were switched on to observe the effect of non-linearities on the particle density. The transverse beam profile was determined by measuring the instantaneous flux of secondary particles produced by a fine wire flying through the beam repeatedly every minute or so. During a typical run, lasting about 30 minutes, protons performed  $10^8$  turns in the Tevatron. Under the influence of sextupoles, the beam increased in size, and the macroscopic density was reduced, since, at microscopic level, void regions were mixed with populated regions. Measurements were performed in the vicinity of the  $2/5$  resonance, with a tune close to 19.4 units. The evolution of the particle distribution was supposed to obey the diffusion equation:

$$\frac{\partial p(J,t)}{\partial t} = \frac{\partial}{\partial J} \left( D(J) \frac{\partial p(J,t)}{\partial J} \right). \quad (75)$$

Here  $p(J,t)$  is the distribution function, normalized to the number of particles  $N(t)$  that survive at time  $t$ , measured by a current transformer, and  $D(J)$  is an amplitude-dependent diffusion coefficient to be determined by fitting with the experimental data given by the wire-scanner profile monitor.

The model of diffusive evolution is based on a four-parameter expression for the diffusion coefficient:

$$D(J) = \begin{cases} D_0 & \text{for } J < J_0 \\ D_0 + d_0(J - J_0)^i & \text{for } J \geq J_0 \end{cases} \quad (76)$$

The most important parameter is  $J_0$  which can be interpreted as the phase space radius inside which the non-linear dynamical effects are negligibly small. The parameter  $D_0$  represents a residual uniform diffusion acting on all particles, that will eventually be caused by external noise. In the experimental fitting,  $D_0$  is arbitrarily allowed to vary from configuration to configuration. The increase of diffusion rate above  $J_0$  is parametrized by  $d_0$  and  $i$ .

Models of profile evolution are computed by solving Eq. (75) with the diffusion coefficient of Eq. (76), with boundary conditions that forbid particle depletion at the origin and force the absence of particles above the mechanical aperture.

The hollow distribution extends over a small annular surface of the phase space. The diffusion coefficient in Eq. (76) is therefore well determined by experimental fits only in the filled area of the phase space. The extrapolation into regions that are not populated experimentally is clearly invalid.

During the experiment the attempt was made to bracket  $J_0$  by preferentially populating a low-diffusion region in one run and a high-diffusion region in the other. The data collection grid was quite limited for operational reasons.

The experimental fit of  $J_0$  was compared with the stability limit for particle motion estimated with element-by-element computer tracking simulations over a quite small number of turns. The ratio between computed short-term dynamic aperture and the experimental boundary for diffusion is consistently equal to about 2. As a rule of thumb, based on this ratio, the realistic value of the dynamic aperture is about a factor of 2 smaller than the optimistic value based on fast numerical estimates.

#### 4.4 Comparison of the SPS and the Tevatron experimental results

There are three common issues, relevant for non-linear dynamics in particle accelerators, that have been addressed by the experiments at CERN and at FNAL.

The first issue deals with relatively simple dynamical quantities like tune-shift with the amplitude and smear, and refers to a time scale that influences the short-term stability. In the two machines, the experimental results concerning these issues are very clean, and the predictability of analytical and numerical estimates is in general quite good.

The second issue concerns the diffusion induced by sextupoles, the time scale of which is quite large. The common result of the two experiments is that the long-term stability depends heavily upon the choice of the working point and the vicinity of low-order resonances. The reproducibility of experimental data is difficult to achieve and requires a large effort to restore identical working conditions. The numerical models give a satisfactory level of predictability, in general better than 30%, provided that most of the imperfections, like finite closed-orbit, linear coupling, power supply ripple, are correctly accounted for. Predictions in general require large computational power. The effort of understanding predictability was mostly done at the SPS, whilst at the Tevatron the construction of an analytical model of diffusion was of the highest concern.

The third issue points out the effect of tune modulations on long-term stability. It was addressed by substantially different methods in the two machines. At CERN, the local diffusion coefficient was measured with a quite direct method, using the technique of collimation retraction. Working points in the vicinity of 2-D resonances that couple the two transverse degrees of freedom were explored. The investigation of the influence of modulation strength and tune was empirically inspired by the overlap criterion. Predictions were based on brute-force simulation techniques. At FNAL, the phenomenon was studied with particles trapped in 1-D horizontal resonance islands. The predictions were based on a simple analytical model, based on Hamilton's equations. Surprisingly enough, the two approaches concluded with empirical recipes that fix to the same value, i.e. a few parts in  $10^{-5}$ , the maximum tolerable tune ripple in hadron colliders.

### 5. CONCLUSION

The concept of dynamic aperture is fundamental for single-particle, non-linear beam-dynamics in hadron accelerators. Mature analytical approaches are available to examine it, based on highly sophisticated mathematical methods that describe Hamiltonian systems and the resonant phenomena relative to them. The most enlightening result is the KAM theorem that, roughly speaking, demonstrates the possible coexistence of stable trajectories and chaotic layers in the phase space of non-integrable Hamiltonian systems. The analysis of the Lyapunov coefficient and the Chirikov criterion of overlapping resonances are crucial in the identification of chaos. And finally, the perturbative theory of maps makes available algorithmic rules to compute higher-order contributions to dynamical quantities.

However, our theoretical understanding is, at present, insufficient for practical applications. Therefore, heuristic approaches have been invented, based on extensive simulations with computer programs, to evaluate the stability of the motion in accelerators. They are very useful for accelerator design and performance evaluations, but they are often specific to the particular accelerator under investigation.

Experiments intended to reproduce in a controlled fashion the non-linear behaviour of particle motion have been intensively pursued for several years in various laboratories on both sides of the Atlantic. We have been able to observe effects of non-linear resonances, onset of

chaos and diffusive motion, that are, to a large extent, in agreement with analytical or numerical expectations, once the unavoidable imperfections which are present in the real machine are correctly considered.

## **ACKNOWLEDGEMENTS**

I wish to thank E. J. Wilson, the head of the CERN Accelerator School, for providing me with the motivation to write this lecture, M. Giovannozzi for his most enlightening discussions on this topic, E. Todesco, F. Schmidt and J. Gareyte for carefully reading the original manuscript, and the staff of the Desktop Publishing Service.

## REFERENCES

- [1] G. D. Birkhoff, *Dynamical Systems* (American Mathematical Society, New York, 1927).
- [2] H. Poincaré, *Les Méthodes nouvelles de la Mécanique céleste* (Gauthier-Villars, Paris, 1892).
- [3] A. Chao, *Recent Efforts on Non-Linear Dynamics*, SSCL-Prep. 132 Rev. 1 (1992).
- [4] A. Schoch, *Theory of Linear and Non-Linear Perturbations of Betatron Oscillations in Alternating Gradient Synchrotrons*, CERN 57–21 (1958).
- [5] R. D. Ruth, *Single Particle Dynamics in Circular Accelerators*, SLAC-PUB-4103 (1985).
- [6] H. Mais, *Non-Linear Problems in Accelerator Physics* (Inst. Phys. Conf. Ser. No. 131, 1992) p. 1.
- [7] E.D. Courant and H. S. Snyder, *Theory of the Alternating-Gradient Synchrotron*, Ann. Phys. (N.Y.) **3** (1958) 1–48.
- [8] V. I. Arnold, *Mathematical Methods of Classical Mechanics* (Springer, New York, 1978).
- [9] G. Guignard, *A General Treatment of Resonances in Accelerators*, CERN 78–12 (1978).
- [10] B.V. Chirikov, *Universal Instability of Many-Dimensional Oscillator Systems*, Phys. Rep. **52** (1979) 263–379.
- [11] M. Hénon, *Numerical Study of Quadratic Area-Preserving Mappings*, Q. Appl. Math. **27** (1969) 291.
- [12] M. Giovannozzi, *Analysis of the Stability Domain for the Hénon Map*, Phys. Lett. **A182** (1993) 255.
- [13] K.G. Steffen, *High Energy Beam Optics* (Interscience, New York, 1965).
- [14] E. Lohrmann and P. Wilhelm, *Rounding Errors in Beam Tracking Calculations*, Part. Accel. **19** (1986) 99.
- [15] H. Grote and C. Iselin, *The MAD Program*, CERN/SL/90–13 (AP) Rev. 3 (1993).
- [16] F. Schmidt, *SIXTRACK version 1.1*, CERN/SL/AP 91–52 (1991).
- [17] Y. Yan, *Applications of Differential Algebra to Single-Particle Dynamics in Storage Rings*, SSCL-500 (1991).
- [18] E. Forrest et al., *The Modern Approach to Single-Particle Dynamics for Circular Rings* (AIP Conf. Proc. No. 292, Upton, 1992) p. 417.
- [19] M. Berz, *Differential Algebraic Description of the Beam Dynamics to Very High Order*, Part. Accel. **24** (1989) 109.
- [20] A. Bazzani et al., *Normal Forms for Hamiltonian Maps and Non-Linear Effects in a Particle Accelerator*, Nuovo Cim. **102 B**, No. 1 (1988) 51–80.
- [21] A.J. Dragt et al., *Lie Algebraic Treatment of Linear and Non-Linear Beam Dynamics*, Ann. Rev. Nucl. Part. Sci. **38** (1988) 455.

- [22] E. Forrest, J. Irwin and M. Berz, *Normal Forms Methods for Complicated Periodic Systems*, Part. Accel. **24** (1989) 91.
- [23] A. Bazzani, E. Todesco, G. Turchetti and G. Servizi, *A Normal Form Approach to the Theory of Non-Linear Betatron Motion*, CERN 94-02 (1994).
- [24] A. Bazzani, M. Giovannozzi, G. Servizi, E. Todesco and G. Turchetti, *Resonant Normal Forms, Interpolating Hamiltonians and Stability Analysis of Area Preserving Maps*, Physica **D64** (1993) 66–97.
- [25] W. Scandale, F. Schmidt and E. Todesco, *Compensation of the Tune-Shift in the LHC, Using the Normal Form Techniques*, Part. Accel. **35** (1991) 53.
- [26] R. Kleiss, F. Schmidt and F. Zimmermann, *The Use of Truncated Taylor Maps in Dynamic Aperture Studies*, Part. Accel. **41** (1993) 117.
- [27] A.M. Lyapunov, *Stability of Motion* (Academic Press, New York, 1966).
- [28] F. Schmidt, F. Willeke and F. Zimmermann, *Comparison of Methods to Determine Long-Term Stability in Proton Storage Rings*, Part. Accel. **35** (1991) 249.
- [29] A. Chao et al., *The Criteria Working Group Summary*, CERN 88-04 (1988) p. 152.
- [30] Z. Guo, T. Risselada and W. Scandale, *Dynamic Aperture of the CERN-LHC with Injection Optics*, Proc. 5th Advanced ICFA Beam Dynamics Workshop on Effects of Errors in Accelerators, their Diagnosis and Corrections, Corpus Christi, 1991, Ed. A.W. Chao (AIP Conf Proc., No. 255, New York, 1992) p. 50.
- [31] F. Galluccio and F. Schmidt, *Towards a Better Understanding of Slow Particle Loss in the Large Hadron Collider*, Proc. 5th Advanced ICFA Beam Dynamics Workshop on Effects of Errors in Accelerators, their Diagnosis and Corrections, Corpus Christi, 1991, Ed. A.W. Chao (AIP Conf Proc., No. 255, New York, 1992) p. 86.
- [32] M. Bassetti, J.P. Koutchouk and W. Scandale, A. Verdier, *Optimisation of the LHC Lattice and Chromaticity*, IEEE PAC 87, Washington, 1987 (IEEE, New York, 1987) p. 1284.
- [33] P. Schmüser, *Field Quality Issues in Superconducting Magnets*, IEEE PAC 91, San Francisco, 1991 (IEEE New York, 1991) p. 37.
- [34] M. Giovannozzi and F. Schmidt, *General Normal Forms Procedure to Correct Tune-Shift and Non-Linear Chromaticity for Large Accelerators like the LHC*, these proceedings.
- [35] D. Neuffer, *Multipole Correction in Large Synchrotrons*, CERN 88-04 (1988) p. 179.
- [36] *Design Study of the Large Hadron Collider (LHC)*, CERN 91-03 (1991) p. 115.
- [37] R. Gluckstern and S. Ohnuma, *Reduction of Sextupole Distortion by Shuffling Magnets in Small Groups*, IEEE PAC 85, Vancouver, 1985 (IEEE, New York, 1985) p. 2315.
- [38] F. Willeke, *A Magnet Ordering Procedure for the HERA Electron-Proton Collider*, DESY-HERA 87-12 (1987).
- [39] W. Scandale and L. Wang, *Installing Two-in-One LHC Magnets in Ordered Sequence*, CERN SPS 89-41 (AMS) (1989).

- [40] S.Y. Lee et al., *Experimental Determination of a Non-Linear Hamiltonian in a Synchrotron*, Phys. Rev. Lett. **67** (1991) 3768.
- [41] D.D. Caussyn, et al., *Experimental Studies of Non-Linear Beam Dynamics*, Phys. Rev. **A46** (1992) 7942.
- [42] M. Ellison, *Driven Response of the Synchrotron Motion of a Beam*, Phys. Rev. Lett. **70** (1993) 591.
- [43] J.Y. Liu et al., *Determination of the Linear Coupling Resonance Strength Using 2-D Invariant Tori*, Phys. Rev. **E49** (1994) 2347.
- [44] L. Evans, J. Gareyte, A. Hilaire, W. Scandale and L. Vos, *The Non-Linear Dynamic Aperture Experiment in the SPS*, EPAC 88, Rome, 1988 (World Scientific, Singapore, 1989) p. 619.
- [45] J. Gareyte, H. Hilaire and F. Schmidt, *Dynamic Aperture and Long Term Stability in the Presence of Strong Sextupoles in the CERN SPS*, PAC 89, Chicago, 1989 (IEEE, New York, 1989) p. 1376.
- [46] A. Burns et al., *The BOSC Project*, EPAC 90, Nice, 1990 (Editions Frontières, Gif-sur-Yvette, 1990) p. 803.
- [47] D. Brandt, E. Brouzet, A. Faugier, F. Galluccio, J. Gareyte, W. Herr, A. Hilaire, W. Scandale, F. Schmidt and A. Verdier, *Influence of the Power Supply Ripple on the Dynamic Aperture of the SPS in the Presence of Strong Non-Linear Fields*, EPAC 90, Nice, 1990 (Editions Frontières, Gif-sur-Yvette, 1990) p. 1438.
- [48] X. Altuna et al., *The 1991 Dynamic Aperture Experiment at the CERN SPS*, Proc. 5th Advanced ICFA Beam Dynamics Workshop on Effects of Errors in Accelerators, their Diagnosis and Corrections, Corpus Christi, 1991, Ed. A.W. Chao (AIP Conf. Proc., No. 255, New York, 1992) p. 355.
- [49] T. Linnecar and W. Scandale, *Continuous Tune Measurement Using the Schottky Detector*, PAC 83, Santa Fe, 1983 (IEEE, New York, 1983) p. 2185.
- [50] D.A. Edwards and M.J. Syphers, *An Overview of the Experiment E778*, CERN 88-04, (1988) p. 95.
- [51] A. Chao et al., *Experimental Investigation of Non-Linear Dynamics in the Fermilab Tevatron*, Phys. Rev. Lett. **61** (1988) 2752.
- [52] S.G. Peggs, *Hamiltonian Theory of the E778 Non-Linear Dynamics Experiment*, CERN 88-04 (1988) p. 131.
- [53] T. Satogata et al., *Driven Response of a Trapped Particle Beam*, Phys. Rev. Lett. **68** (1992) 1838.
- [54] T. Chen et al., *Measurements of a Hamiltonian System and their Description by a Diffusive Model*, Phys. Rev. Lett. **68** (1992) 33.